2003-07-11

Identifying the Location of a Sudden Damage in Composite Laminates Using Wavelet Approach

Armaghan Salehian
Worcester Polytechnic Institute

IDENTIFYING THE LOCATION OF A SUDDEN DAMAGE IN COMPOSITE LAMINATES USING WAVELET APPROACH

by

Armaghan Salehian

A Thesis

Submitted to the Faculty

of the

WORCESTER POLYTECHNIC INSTITUTE

In partial fulfillment of the requirements for the

Degree of Master of Science

in

Mechanical Engineering

by

_____

June 2003

APPROVED:

_____

Professor Zhikun Hou, Thesis Advisor

_____

Professor Mikhail Dimentberg, Committee Member

_____

Professor Joseph J. Rencis, Committee Member

_____

Professor John Sullivan Jr., Graduate Committee Representative

ABSTRACT

This study presents a general approach for an inverse problem to locate a sudden structural damage in a plate. The sudden damage is modeled as an impulse load and response data are collected at various sensor locations. In this simulation study the response data were generated by the commercial finite element code ANSYS for three square plates: one is an isotropic plate and made of aluminum and the others are two different composite plates made of graphite-epoxy. All plates are simply supported along all their edges. The responses of these plates to both narrow band and wide band loading were analyzed by a wavelet transform. The wavelet coefficient maps for each type of signal was utilized to estimate the shortest path arrival times of flexural waves resulted from the damage by locating the wavelet coefficient peak values of the response data. Using the dispersion relations of wave propagation based on the Mindlin's plate theory, a set of nonlinear equations were derived to solve this inverse problem and the location of the applied load, which models a structural damage, was determined. The estimated locations for all different types of plates have shown an excellent agreement with the actual location of the impact loads applied.

ACKNOWLEDGEMENTS

My special thanks go to my thesis advisor, Zhikun Hou. His wisdom and direction were instrumental in the preparation of this research. I would like to appreciate the technical insights provided by Professor F.G. Yuan at NCSU and his student Ms. Aihua Lang. I thank all the help of my friend Sia Najafi for providing me with computer facilities. I greatly appreciate Professor John .M. Sullivan for his technical guidance. I would like to thank my friend Adriana Hera for all her help during the completion of this master thesis. Above all I would like to thank my parents for their support and encouragement. They were always there whenever I needed them.

TABLE OF CONTENETS

LIST OF FIGURES

LIST OF TABLES

CHAPTER 1

INTRODUCTION

1.1 Literature Review

Traditionally, dynamic analysis of structures in response to loading can be classified as three basic problems

- given the input and the system parameters, determine the output
- given the system parameters and the output, determine the input
- given the input and the output, determine the system parameters

Problems of the first category are described as direct problems of dynamic analysis while the second type (the load identification problems) and the third type (the system identification problems) are called inverse problems [5].

Inverse problems are quite popular in industry. The inverse problems in composite plates are specially important. Composite materials are widely being used in the aerospace industry and they have many other commercial applications because of their low density, high performance and increased service life. In this study we employ the load identification problem to locate a sudden structural damage modeled by an impulse. This inverse problem becomes specially useful for challenging case that the damage is hidden and can't be detected by visual inspection. Nondestructive tests such as X-Ray, C-Scan and others may partially address the problem but they can be very expensive, quite time consuming and

impractical for big structures. Therefore, inverse methods become promising for detecting the stiffness loss due to delaminations in a structure.

A literature review shows that several approaches are currently available for inverse load identification problems. Doyle [12] determined the contact force during the transverse impact of an isotropic plate from dynamic strain gage measurements through several sensors. The location of an impact in a beam was determined by the same author by using the theory of wave propagation and studying the phase change of experimentally measured strains [7]. Further developments have been done by the same author to incorporate the shear effects of transverse impact in beams [11]. He also investigated a force identification problem from dynamic responses of a bimaterial beam [8]. Another method is represented by him using a frequency domain deconvolution method to determine the location of the force in beam structures [9].

Michaels [26] developed an experimental method to generate oblique forces in plates with known orientations and time history and the recorded signals were analyzed by an iterative deconvolution method to determine the orientations and the time histories of the forces. Ziola and Gorman [38] identified the source location of waves propagating in a thin isotropic plate using a cross-correlation method. Cruz [4] presented a method to determine the location and magnitude of *static* force acting on a plate. He also investigated the responses of a viscoelastic plate to a harmonic force in order to find the location, magnitude and phase of the force [5]. Li used the wavelet approach to solve a load identification problem in

beam structures, she also identified the force-time history of the loading by using neural network method [39]. Gaul and Hurlebas [14] used a wavelet approach in order to solve the inverse load identification problem in isotropic plates. Choi and Chang [6] presented an identification method using distributed built-in sensors for detecting impact of a foreign object on a beam. The identification problem consisted of a system model and a response comparator and the system model characterizes the dynamic response of the structure subject to a known impact force.

1.2 Motivation and objective

The above literature survey shows that intense study has been done in inverse problems. Previous research mainly focuses on beams and isotropic plates. To my knowledge no research has been done in composite plates. The problem in composites becomes challenging because of technical difficulties due to the fiber orientations and variations of wave velocities in different directions. In general any loaded structure can be modeled as a series of springs under tension or compression, when any kind of sudden damage or delaminations happen in the structure, some of the springs fail to tolerate the load and the strain energy stored in them is released in the form of kinetic energy. So the sudden crack becomes a source for the propagating waves. Hence the damage can be modeled by an impulse load. The objective of this study is to simulate a sudden structural

damage by an impulse and solve an inverse load identification problem to locate the modeled damage.

1.3 Organization of Chapters

Chapter 2 mainly deals with the simulation of the response data by ANSYS for two different types of loading and stability conditions of the analysis. In order to locate the damage that can be modeled as an arbitrary impulse load, the Wavelet Transformation is employed in Chapter 3. It is proven that the peak values of the magnitude of the Wavelet Transformation of the measured signals give the arrival times. A summary of the Mindlin's Plate Theory, dispersion relations and how they are employed to locate the damage, are presented in Chapter 4. In this chapter we use the arrival times calculated in Chapter 3 and the group velocities calculated in this chapter to solve a set of nonlinear equations to estimate the location. The conclusion and discussion of the numerical results are presented in Chapter 5.

CHAPTER 2

SIMULATION OF THE RESPONSE DATA

In this chapter the transverse deflection response of a plate to an impulse load, which models sudden structural stiffness loss, is simulated numerically by ANSYS version 7.0, a commercial finite element software package.

2.1 Loading Specifications

In this study, we consider the wave propagation in rectangular isotropic and composite plates for two different types of loading. The first one is a narrow band modulated sinusoidal burst wave form given by:

$$f(t) = P[H(t) - H(t - N_P / f_0)][1 - \cos(2\pi f_0 t / N_P)]\sin(2\pi f_0 t) \quad (2.1)$$

where H(t) is the unit step function, $f_0 = 100KHz, N_P = 5, P = 40N$. This loading is shown in Figure 2-1 and 2-2 in time and frequency domain. The second one is a wide band triangular shape impulse, defined as:

$$f(t) = P[H(t) - H(t - 5\times10^{-5})][1 - (t - 2.5\times10^{-5})\times \text{sign}(t - 2.5\times10^{-5})/2.5\times10^{-5}] \quad (2.2)$$

The waveform and its frequency spectrum are shown in Figures 2-3 and 2-4. The narrow band impulse loading was applied in order to show the non-dispersive characteristics of this type of loading. The definition of the narrow band and wide band refers to the frequency spectrum of the signals and it depends on the ratio of the frequency band width to the central frequency.

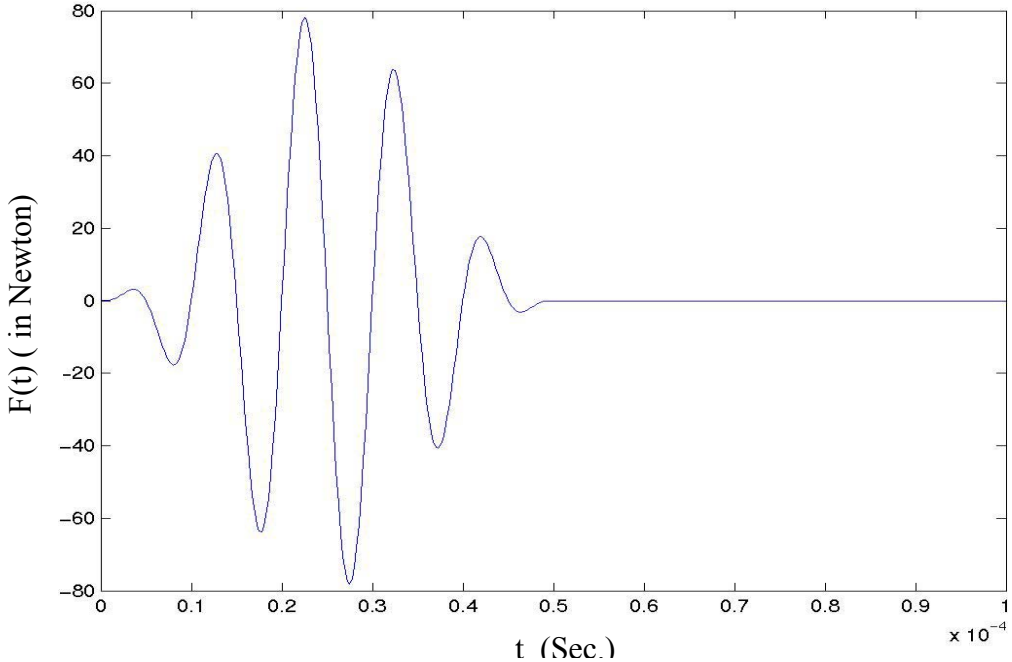

Figure 2-1 Narrow band five peak load

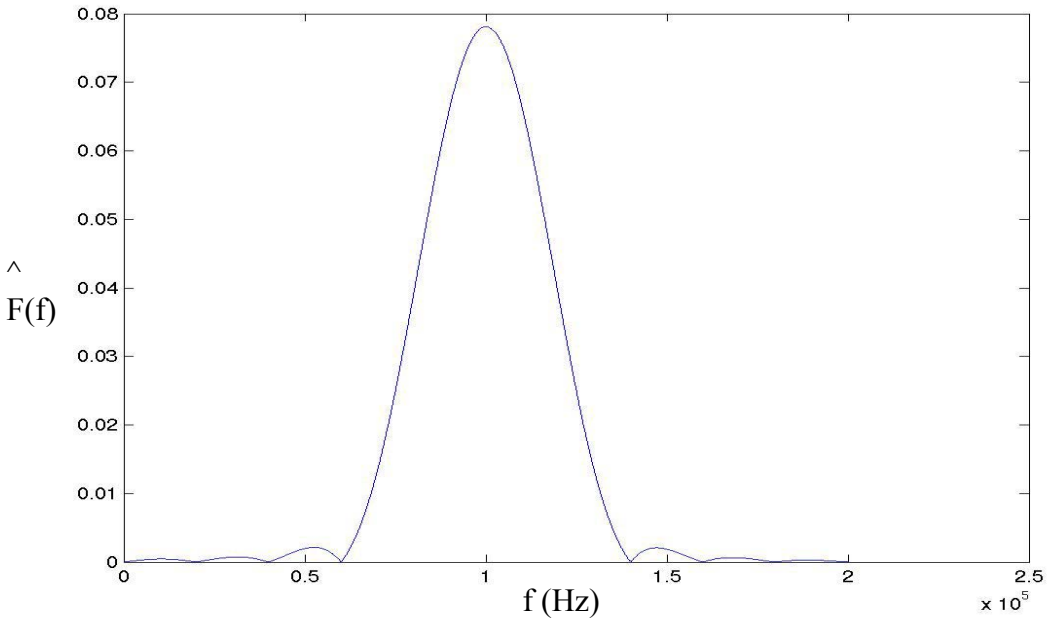

Figure 2-2 Fourier spectrum of the Narrow band load

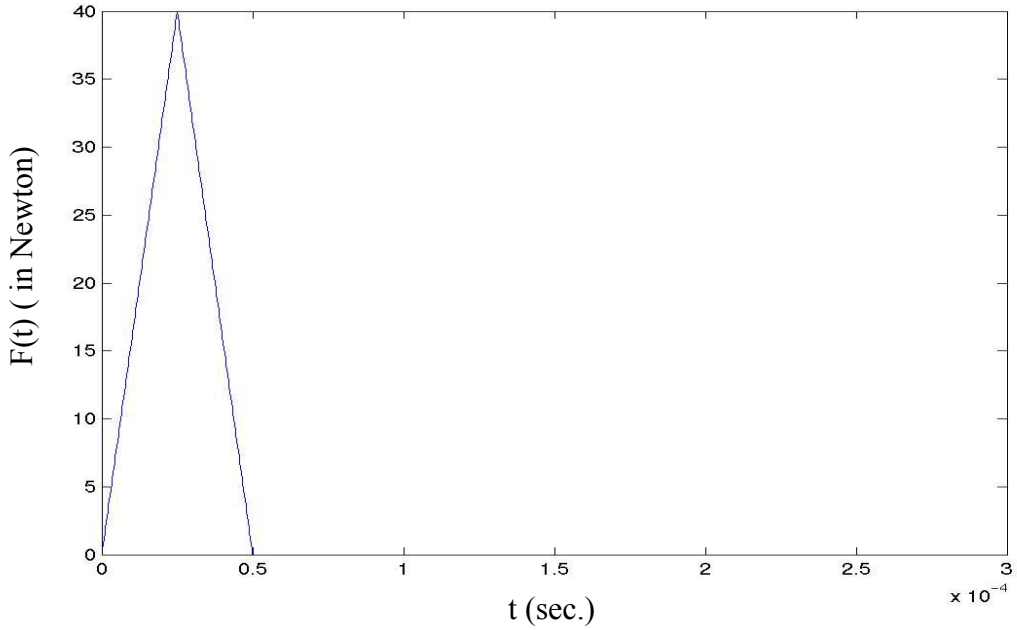

Figure 2-3 Wide band triangular load

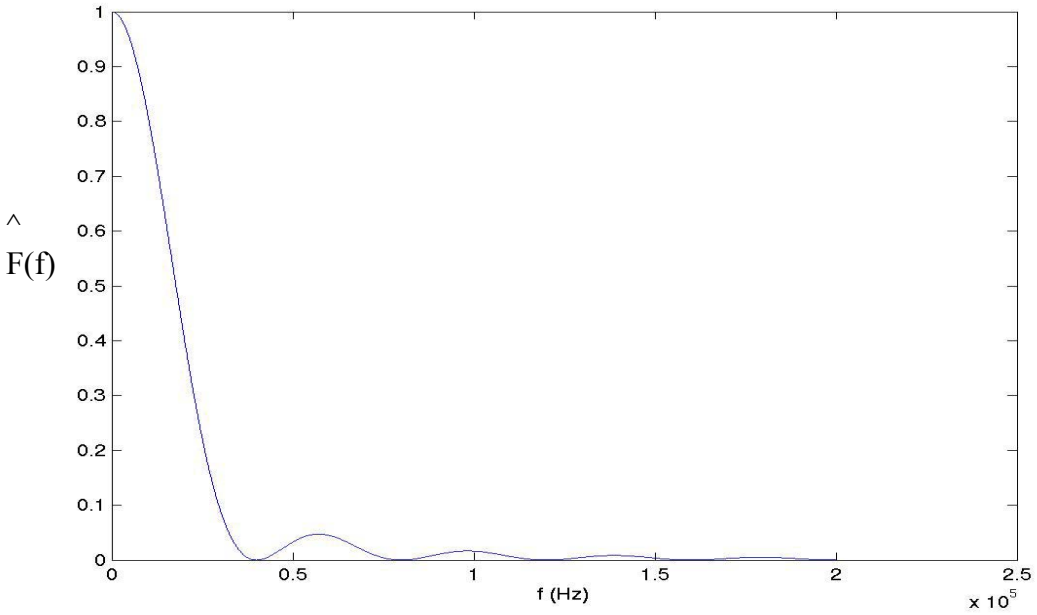

Figure 2-4 Fourier spectrum of the triangular load

2.2 Generation of Simulation Signals

In this study measurement data of structural response are simulated for three square plates simply supported along all their edges: one is isotropic, made of aluminum and others are composite plates made of graphite epoxy. One is a two-layer laminate composite plate with 0^0 and 90^0 orientation of the fibers ([0/+90]), and the other is a three layer composite plate with [+45/0/-45] fiber orientations. The material properties and the geometries of the plates are shown in Tables 2-1 and 2-2 for the aluminum and graphite epoxy plates respectively. Without loss of generality the location of the applied impulse force was selected at x=0.5m, y=0.7m. Codes in ANSYS 7.0 were written to simulate the wave propagation response at several sensor locations. Codes were run on Linux cluster with the following configuration: Workstation at W.P.I., model: Dell Power Edge 2650, dual processor each 2.4 GHz Xeon, 2 GB of RAM 36 GB Hard disk drive, operating system Linux RedHat 7.3.

For each plate, response signals are generated for two different types of loading. Three rectangular plates with the side length of 1m×1m with the material properties shown in the tables were used in this analysis. The finite element mesh size is 5 mm and the sampling period is 0.25 μs. The element used is ANSYS element SHELL99, that consists of 8 nodes with 6 degrees of freedom per node. The total number of the nodes is 120801 and the number of elements is 40000. As we will explain later in this chapter the mesh size and the time step are crucial in stability of the analysis. Figures 2-5 to 2-7 illustrate the simulated response

signals at sensor 1 for each plate. The material properties are presented in Tables 2-1 and 2-2. Without loss of generality, the sensor locations are arbitrarily chosen as defined in Table 2-3. Recording the signals for composite plates is interrupted at a time to avoid boundary reflections. More results for other sensors can be found in Appendix B. In the isotropic plate the wave speed is higher and as we see we get the reflections from the boundary in almost 2.5×10^{-4} (sec.) at sensor 1. Comparing the results of sensor 1 in composite 1 and 2 we see that the amplitude of the signal is bigger for the composite 2 and this is expected due to the fact that the thickness of composite 2 is smaller hence, the mass per unit area swept by the wave is bigger in composite 1. So based on the conservation of energy the amplitude should be smaller. For the narrow band loading in each case we see almost no distortion in the recorded signals and this is also expected because as we will explain later in the Chapter 4 in a narrow band signal the group velocity is almost constant for different frequency contents.

Table 2-1- Material properties of isotropic plate made of aluminum

L_1 (m)	L_2 (m)	h (m)	E (Gpa)	υ	G (GPa)	ρ (Kg/m^3)
1	1	0.0025	72.5	0.3	27.885	2710

Table 2-2 Material properties of composite plate 1[0/+90] and composite plate 2 [+45/0/-45] made of graphite-epoxy

Plate	L_1	L_2	h m	E_1 Gpa	E_2 GPa	E_3 GPa	υ_{12}	υ_{23}	υ_{13}	G_{12} GPa	G_{23} GPa	G_{13} GPa	ρ Kg/m^3
Composite 1	1	1	0.005	138	8.9	8.9	0.3	0.54	0.3	5.17	2.89	5.17	1600
Composite 2	1	1	0.00375	138	8.9	8.9	0.3	0.54	0.3	5.17	2.89	5.17	1600

Table 2-3 Location of the sensors (m)

Sensor / Coordinates	S_1	S_2	S_3
x	0.28	0.78	0.38
y	0.52	0.52	0.92

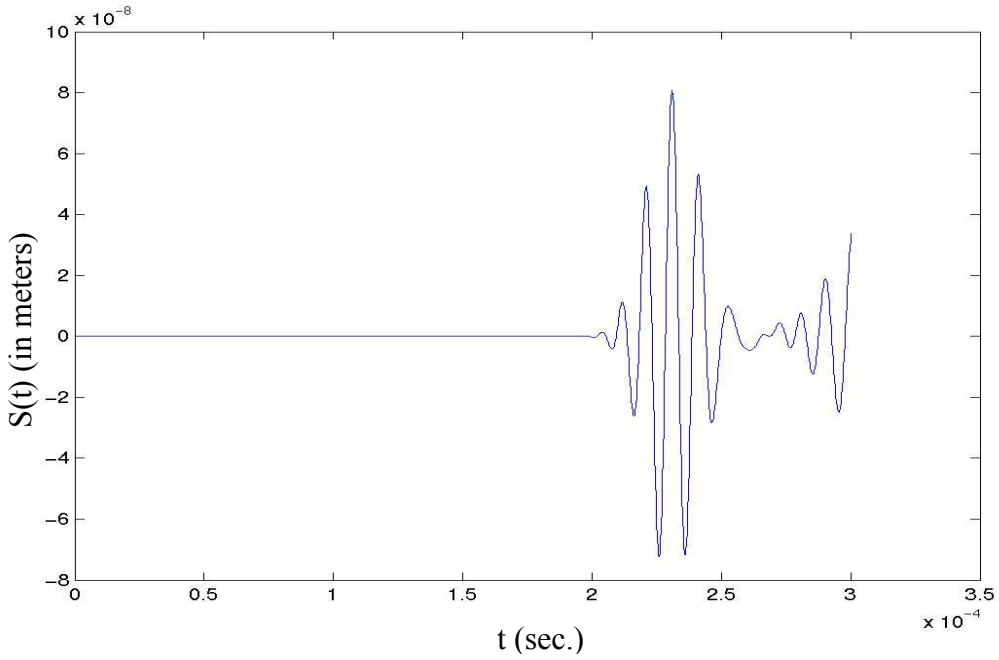

a) narrow band load

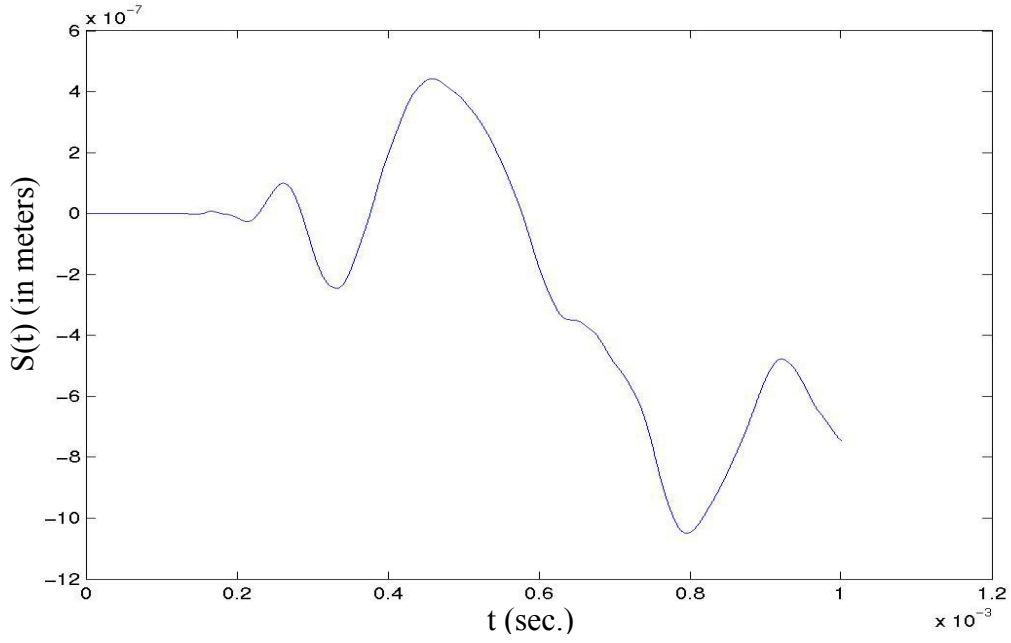

b) wide band load

Figure 2-5 Signal recorded at sensor 1 in isotropic plate

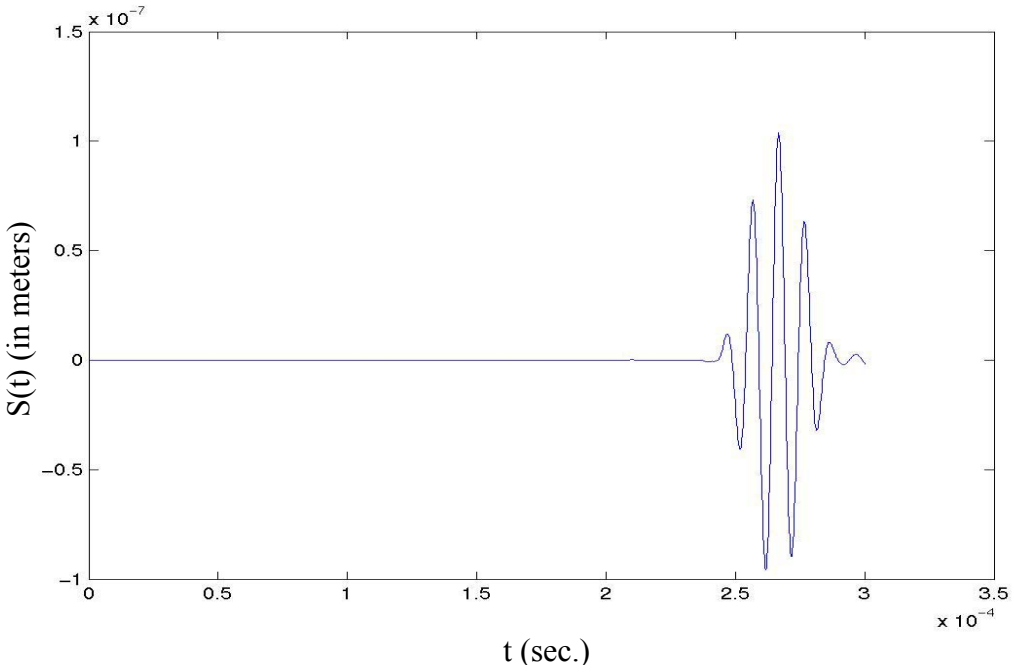

a) narrow band load

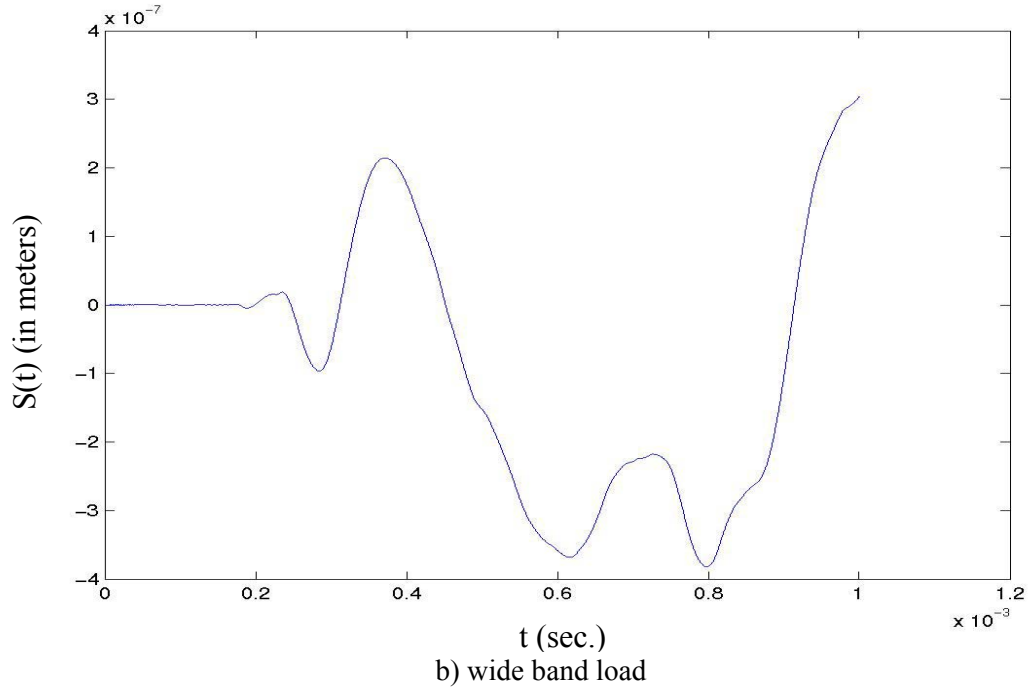

b) wide band load

Figure 2-6 Signal recorded at sensor 1 in composite 1

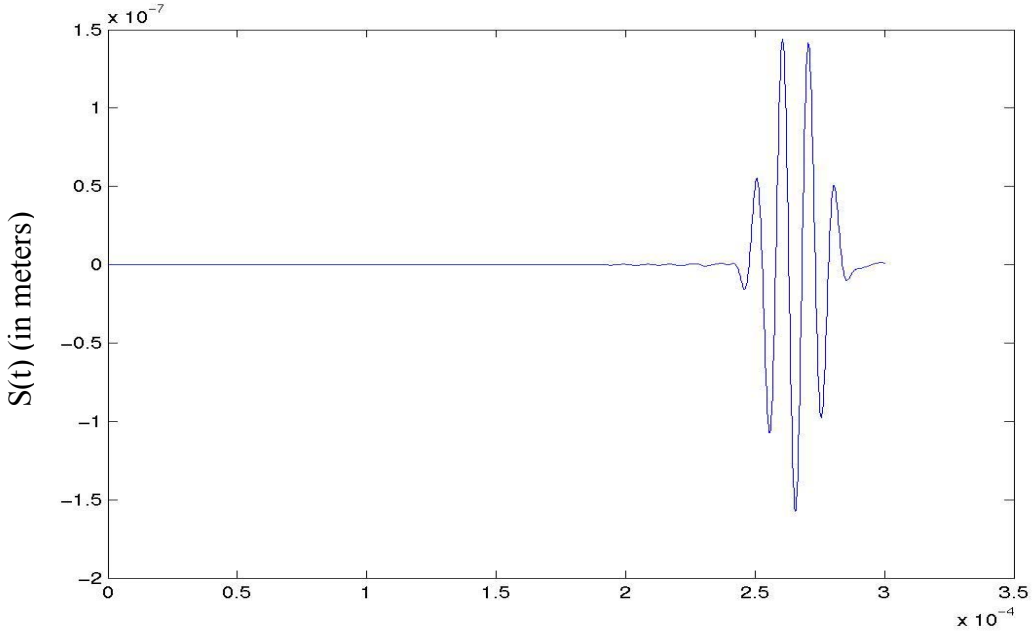

a) narrow band load

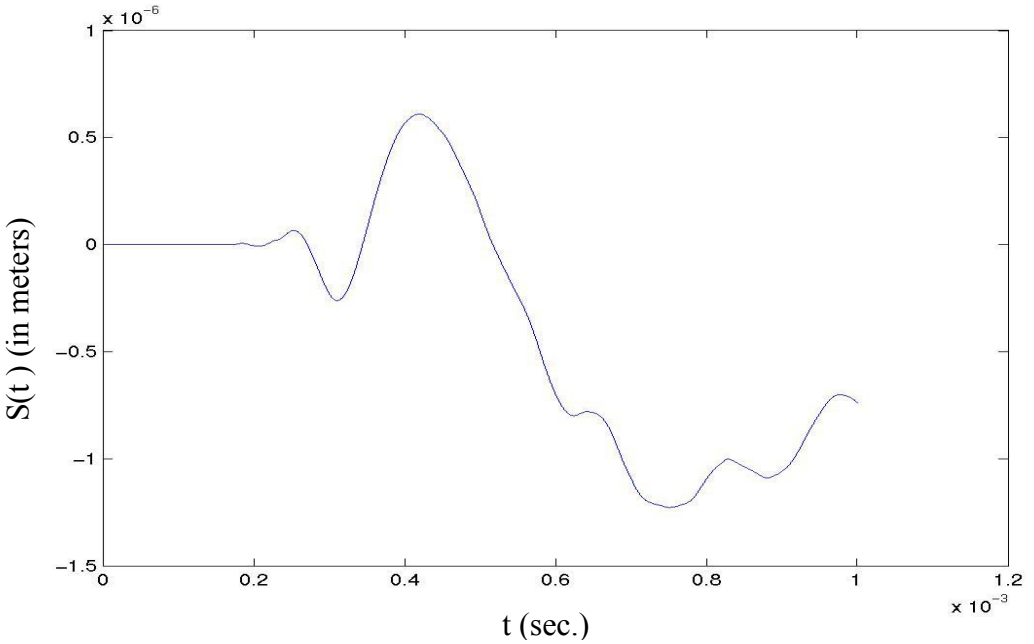

b) wide band load

Figure 2-7 Signal recorded at sensor 1 in composite 2

2.3 Selection of the Time Step for Stability

The selection of time step is quite crucial in this simulation, as suggested by ANSYS the following criteria should be used to get stable numerical results. It has been found that using approximately twenty points per cycle for the highest frequency of interest results in a reasonably accurate solution, or:

$$\Delta t \le \frac{1}{20 f_{\max}} \tag{2.3}$$

where f_{max} is the frequency of the highest flexural mode that contributes to the response and is related to the transverse deflection. To be accurate we consider the first 10 modes in this study.

Table 2-4 The 10^{th} mode natural frequencies and suggested time steps

Plate	Frequency (Hz.)	Suggested Time Step (sec.)
Isotropic	1231	4.05e-5
Composite 1	5003	9.99e-06
Composite 2	3752	1.33e-05

The other condition for stability of analysis is that the time step should be small enough so that the wave can not travel one size of an element at each time step, or:

$$\Delta t \le \frac{l}{C_g} \tag{2.4}$$

where l is the mesh size and C_g is the group velocity of the propagating wave. The maximum group velocity for each of the three plates for the highest frequency considered is 1200m/s. So we have, $\Delta t \le 2.5e-06$ sec.

Also, the time step should be small enough to follow the loading functions. The response tends to lag the applied loads. In case of stepped load, the values as small as $\Delta t \le \frac{1}{180 f}$ may be needed, where f is the highest frequency of the load. In this study, the relation

$$\Delta t \le \frac{1}{40 f} \tag{2.5}$$

was found by trial and error. Finally, the value of 0.25×10^{-6} (sec.) satisfies all of the above conditions.

CHAPTER 3

WAVELET TRANSFORM

3.1 Background of Wavelet Analysis

A wavelet approach is used in this study to find the shortest path arrival time for different frequency contents of the signal. The continuous wavelet transform WT of a function $f(t)$ is defined by:

$$WT_f(a,b) = \frac{1}{\sqrt{a}} \int_{-\infty}^{\infty} f(t) \psi^* \left(\frac{t-b}{a} \right) dt \qquad (3.1)$$

where a>0 and superscript * denotes a complex conjugation. The Kernel function in the WT

$$\psi_{a,b}(t) = \frac{1}{\sqrt{a}} \psi \left(\frac{t-b}{a} \right) \qquad (3.2)$$

is generated by shifting and scaling a mother wavelet $\psi(t)$.

The parameter a represents the scale variable in the WT similar to a frequency variable in the Fourier transform and b is the shift parameter. The scaling is a primary characteristic of the wavelet analysis. In time domain $\psi_{a,b}(t)$ is centered at b with a spread proportional to a. In this study the relation between frequency ω and scale variable 'a' is $\omega = \frac{\omega_0}{a}$, where ω_0 is the central frequency which is the dominant frequency of the mother wavelet. Function $\psi_{a,b}$ can be considered as a window function both in time and frequency domains and we can change the

window size by changing the variable *a* to get the appropriate resolution. This multiresolution is a primary characteristic of the wavelet analysis.

A wavelet function should satisfy several conditions, one is that the mother function should be finite support in time domain or,

$$\lim_{t \to \infty} \psi(t) \to 0 \tag{3.3}$$

Also $\psi(t)$ satisfies the admissibility condition, which means that the following integration should be finite:

$$C_\psi = \int_{-\infty}^{\infty} \frac{\left| \hat{\psi}(\omega) \right|^2}{|\omega|} d\omega < \infty \tag{3.4}$$

where $\hat{\psi}(\omega)$ denotes the Fourier Transform of $\psi(t)$.

The Garbor function, defined as

$$\psi_g(t) = \frac{1}{\sqrt[4]{\pi}} \sqrt{\frac{\omega_0}{\gamma}} \exp\left(-\frac{(\omega_0/\gamma)^2}{2} t^2 \right) \exp(i\omega_0 t) \tag{3.5}$$

is employed as the mother wavelet in this study because on its properties of good resolution in both time and frequency domains [15]. The Garbor function Fourier transform is:

$$\hat{\psi}_g(\omega) = \frac{\sqrt{2\pi}}{\sqrt[4]{\pi}} \sqrt{\frac{\gamma}{\omega_0}} \exp[-\frac{(\gamma/\omega_0)^2}{2} (\omega - \omega_0)^2] \tag{3.6}$$

Following [15] the positive constants γ and ω_0 are set as: $\gamma = \pi\sqrt{\frac{2}{\ln 2}} = 5.336$ and $\omega_0 = 2\pi$. The Garbor function may be considered as a Gaussian window

function centered at t=0 in the time domain and at $\omega = \omega_0$ in the frequency domain. This function is shown in both time and frequency domains in Figures 3-1 and 3-2 respectively. The dotted and solid lines in the Figure 3-1 show the real and imaginary parts respectively.

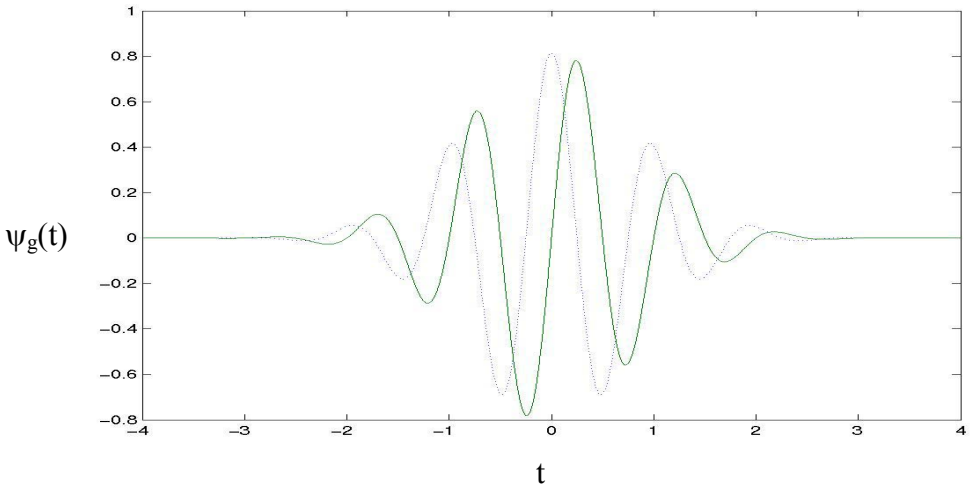

Figure 3-1 Garbor function real and imaginary parts

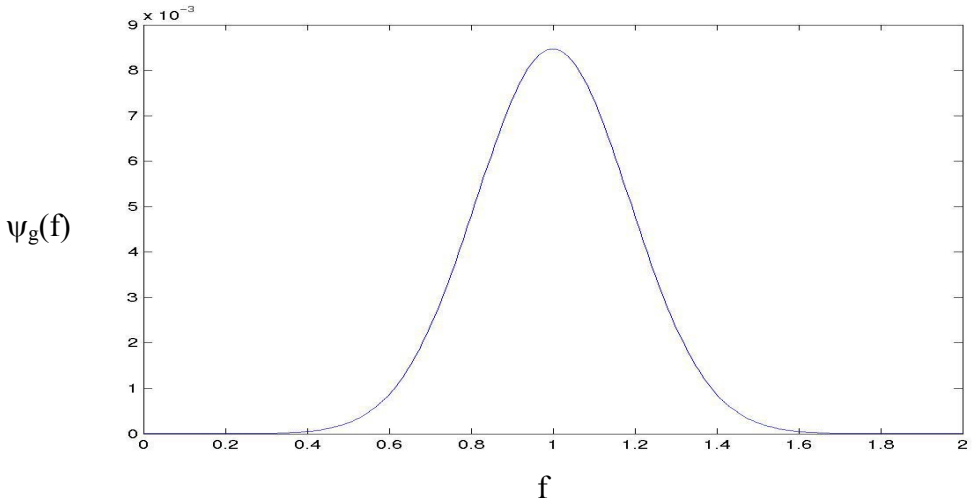

Figure 3-2 Frequency spectrum of the Garbor function

We can see that if $\hat{\psi}(\omega)$ is centered at $\omega = \omega_0$ and $\psi(t)$ is centered at t=0 $\hat{\psi}_{a,b}(\omega)$ is centered at $\omega = \frac{\omega_0}{a}$ in frequency domain and centered at b in time domain . Using the definition of Fourier transform, we have:

$$\hat{\psi}(\omega) = \int_{-\infty}^{+\infty} \psi(t) e^{-i\omega t} dt$$

$$\hat{\psi}_{a,b}(\omega) = \int_{-\infty}^{+\infty} \frac{1}{\sqrt{a}} \psi(\frac{t-b}{a}) e^{-i\omega t} dt \qquad (3.7)$$

assuming that,

$$\frac{t-b}{a} = \tau \qquad (3.8)$$

we have

$$\hat{\psi}_{a,b}(\omega) = \frac{1}{\sqrt{a}} \int_{-\infty}^{+\infty} \psi(\tau) e^{-i\omega(a\tau+b)} a d\tau = \sqrt{a}\, \hat{\psi}(a\omega) e^{-i\omega b} \qquad (3.9)$$

So $\hat{\psi}(a\omega)$ gets its peak value at $\frac{\omega_0}{a}$.

3.2 Group and Phase Velocities of Propagating Waves

In this section the concept of the group velocities of waves is presented. As the arrival times defined by the Wavelet Transform are related to the group velocities. In general, the strains at various points in response to a wideband load consist of a range of frequencies, so we can assume the wave propagating in an arbitrary direction for example x as follow:

$$u(x,t) = \sum_{j=1}^{\infty} C_j e^{-i(k_j x - \omega_j t)} \tag{3.10}$$

where k_j is the wave number corresponding to each frequency ω_j of the j[th] harmonic component. Consider the two harmonic waves of equal unit amplitude and of slightly different frequencies ω_1 and ω_2 propagating in the x-direction [18].

$$u(x,t) = e^{-i(k_1 x - \omega_1 t)} + e^{-i(k_2 x - \omega_2 t)} \tag{3.11}$$

Introducing

$$\begin{aligned} &(k_1 + k_2)/2 = k_c, (k_1 - k_2)/2 = \Delta k, \\ &(\omega_1 + \omega_2)/2 = \omega_c, (\omega_1 - \omega_2)/2 = \Delta\omega \end{aligned} \tag{3.12}$$

Equation (3.10) can be written as [18]:

$$\begin{aligned} u(x,t) &= e^{-i\left((k_c + \Delta k)x - (\omega_c + \Delta\omega)t\right)} + e^{-i\left((k_c - \Delta k)x - (\omega_c - \Delta\omega)t\right)} \\ &= e^{-i(k_c x - \omega_c t)}[e^{-i\Delta k x + i\Delta\omega t} + e^{+i\Delta k x - i\Delta\omega t}] \\ &= 2\cos(\Delta k x - \Delta\omega t) e^{-i(k_c x - \omega_c t)} \end{aligned} \tag{3.13}$$

This represents a carrier with frequency ω_c and a phase velocity ω_c / k_c and the modulation $\cos(\Delta k x - \Delta\omega t)$ with frequency $\Delta\omega$ and propagating velocity of $\Delta\omega / \Delta k$. The wave may be described as a succession of moving beats (or groups, or wave packets). The carrier velocity is c_p while the group velocity is the velocity of the modulation and is c_g. The situation is represented in Figure 3-3 where we see a succession of wavelets (ω, k) with variable amplitude $(\Delta\omega, \Delta k)$. If we do not pay attention to the detailed motion and observe only the average

amplitude distribution, we verify that the amplitude curve moves forward with the group velocity c_g.

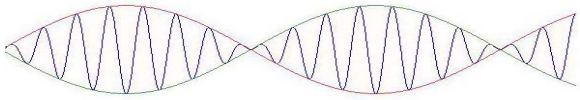

Figure 3-3 Schematic view of a wave superposed of two single frequencies

Looking more carefully at the detailed vibrations, we may see the wavelets moving within the envelope with their own velocity c_p. We distinguish two different cases [24]:

1) $c_g > c_p$ The wavelets are building up in front of the group and disappearing in the rear end of the group.

2) $c_p > c_g$ The wavelets are building up at the back end of the group, progressing through the group and disappearing in the front.

It is worth to point out that the term of dispersive wave is attributed to the wave of which phase velocity is dependent upon ω, on the other hand the phase velocity changes with ω, and since different frequency contents in wave travel at different speeds, the wave is distorted while traveling, however, a non dispersive wave always keeps the same shape because all different frequency contents travel at the same velocity.

3.3 Determining the arrival time Using Wavelet Transform

When the Garbor wavelet is used as the mother wavelet, the WT of $u(x,t)$ is in (3.11) given by:

$$WT_u(x,a,b) = \frac{1}{\sqrt{a}}\int_{-\infty}^{\infty}\psi_g\left(\frac{t-b}{a}\right)[e^{-i(k_1x-\omega_1t)}]dt + \frac{1}{\sqrt{a}}\int_{-\infty}^{\infty}\psi_g\left(\frac{t-b}{a}\right)[e^{-i(k_2x-\omega_2t)}]dt$$

$$= \frac{1}{\sqrt{a}}e^{-ik_1x}\int_{-\infty}^{\infty}\psi_g\left(\frac{t-b}{a}\right)e^{i\omega_1t}dt + \frac{1}{\sqrt{a}}e^{-ik_2x}\int_{-\infty}^{\infty}\psi_g\left(\frac{t-b}{a}\right)e^{i\omega_2t}dt \tag{3.14}$$

assuming,

$$\eta = \frac{t-a}{b} \tag{3.15}$$

we have,

$$= \frac{1}{\sqrt{a}}e^{-ik_1x}\int_{-\infty}^{\infty}\psi_g(\eta)e^{i\omega_1(\eta a+b)}ad\eta + \frac{1}{\sqrt{a}}e^{-ik_2x}\int_{-\infty}^{\infty}\psi_g(\eta)e^{i\omega_2(\eta a+b)}ad\eta$$

$$= \sqrt{a}e^{-i(k_1x-\omega_1b)}\int_{-\infty}^{\infty}\psi_g(\eta)e^{i\omega_1\eta a}d\eta + \sqrt{a}e^{-i(k_2x-\omega_2b)}\int_{-\infty}^{\infty}\psi_g(\eta)e^{i\omega_2\eta a}d\eta$$

$$= \sqrt{a}e^{-i(k_1x-\omega_1b)}\hat{\psi}_g(a\omega_1) + \sqrt{a}e^{-i(k_2x-\omega_2b)}\hat{\psi}_g(a\omega_2) \tag{3.16}$$

Assuming:

$$\phi_1 = \omega_1b - k_1x\,;\phi_2 = \omega_2b - k_2x \tag{3.17}$$

We have,

$$\left|WT_u(x,a,b)\right| = \sqrt{a}\left|\hat{\psi}_g(a\omega_1)e^{i\phi_1} + \hat{\psi}_g(a\omega_2)e^{i\phi_2}\right|$$

$$= \sqrt{a}\left|(\hat{\psi}_g(a\omega_1))^2 + (\hat{\psi}_g(a\omega_2))^2 + 2\hat{\psi}_g(a\omega_1)\hat{\psi}_g(a\omega_2)\cos(\phi_1 - \phi_2)\right|^{1/2}$$

$$= \sqrt{a}\left|(\hat{\psi}_g(a\omega_1))^2 + (\hat{\psi}_g(a\omega_2))^2 + 2\hat{\psi}_g(a\omega_1)\hat{\psi}_g(a\omega_2)\cos(\Delta\omega b - \Delta k x)\right|^{1/2}$$

(3.18)

We can assume:

$$\hat{\psi}_g(a\omega_1) \cong \hat{\psi}_g(a\omega_2) \cong \hat{\psi}_g(a\omega_c) \tag{3.19}$$

so we get:

$$\left|WT_u(x,a,b)\right| = \sqrt{a}\,\hat{\psi}_g(a\omega_c)[1 + 2.\cos(\Delta\omega b - \Delta k x)] \tag{3.20}$$

Hence, by finding the peak values of the $\hat{\psi}_g(a\omega_c)$ and $[1+\cos(\Delta\omega b - \Delta k x)]$, we get the peak value of the wavelet coefficient. As mentioned before the $\hat{\psi}_g(a\omega_c)$ is centered at $\omega = \frac{\omega_0}{a}$, also the term in the brackets will have its maximum value at $\frac{\Delta\omega}{\Delta k} = \frac{x}{b}$, or,

$$c_g = \frac{x}{b} \tag{3.21}$$

It is concluded that the time shift b which maximizes the *WT* coefficient should be the arrival time of the envelope of the wave at circular frequency ω related to the scale *a* by $\omega = \frac{\omega_0}{a}$ for coordinate x. However, since we have the signal in a

discretized form parameter a should be scaled by Δt i.e. the sampling period of the signals in Matlab codes.

3.4 Results for arrival times and Recorded Signals

Tables 3-1 and 3-2 show the arrival times found by the map of the wavelet transform of the recoded signals at each sensor for composite plates. The wavelet transform map of the recorded signals at sensor 1 are presented in Figures 3-4 to 3-6 for two types of loading. The red regions are related to the highest magnitude of the WT. A complete listing of the recorded signals for all the sensors and different types of plates and loading is given in Appendix A. Looking at the Figures of the narrow band, we see that figures have symmetry around a vertical axis. This means that the *'b'* value which maximizes the wavelet coefficient is almost the same for different scales. Or different frequency contents of the signal arrive at the same time which is expected from a narrow bad load. As we also see in the tables the arrival times get smaller when the frequency increases, and this is an expected fact because high frequency components of a signal travel faster.

Table 3-1 Estimated arrival times for different frequency contents to sensors in composite plate-1 (10^{-4}sec.)

Load	Wide band Load					Narrow Band
Freq / Sensor	9.5 (KHz)	15.9 (KHz)	23.8 (KHz)	31.8 (KHz)	39.8 (KHz)	100.2 (KHz)
S_1	2.950	2.850	2.720	2.620	2.465	2.315
S_2	3.420	3.332	3.055	3.005	2.790	2.625
S_3	2.596	2.500	2.440	2.360	2.230	2.100

Table 3-2 Estimated arrival times for different frequency contents to sensors in composite plate-2 (10^{-4}sec.)

Load	Wide Band Load					Narrow Band
Freq / Sensor	9.5 (KHz)	15.9 (KHz)	23.8 (KHz)	31.8 (KHz)	39.8 (KHz)	100.2 (KHz)
S_1	3.565	3.120	2.850	2.735	2.555	2.305
S_2	4.160	3.505	3.190	3.111	2.880	2.585
S_3	3.140	2.855	2.60	2.480	2.330	2.115

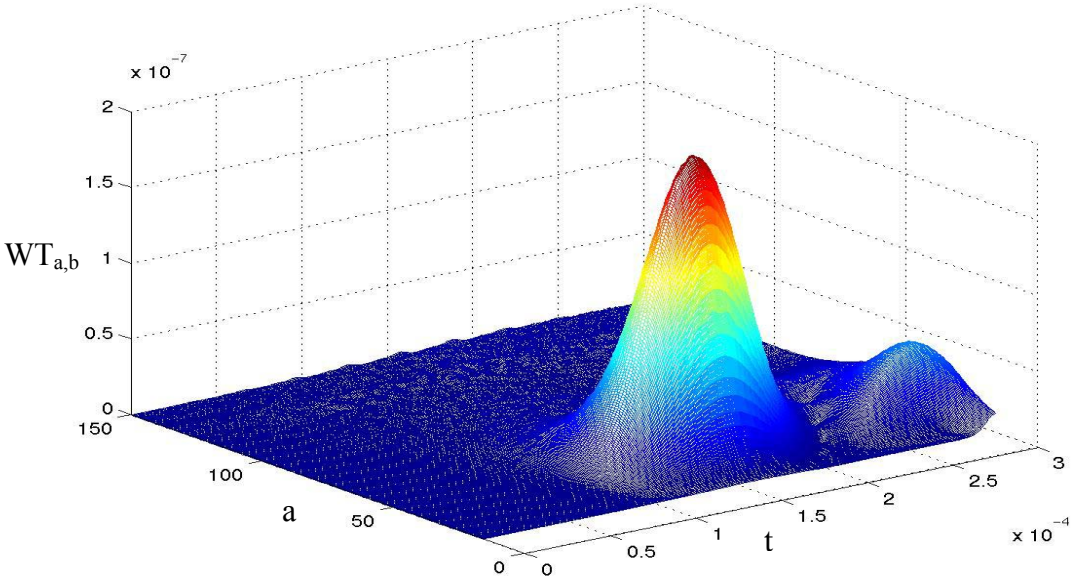

a) Narrow band load

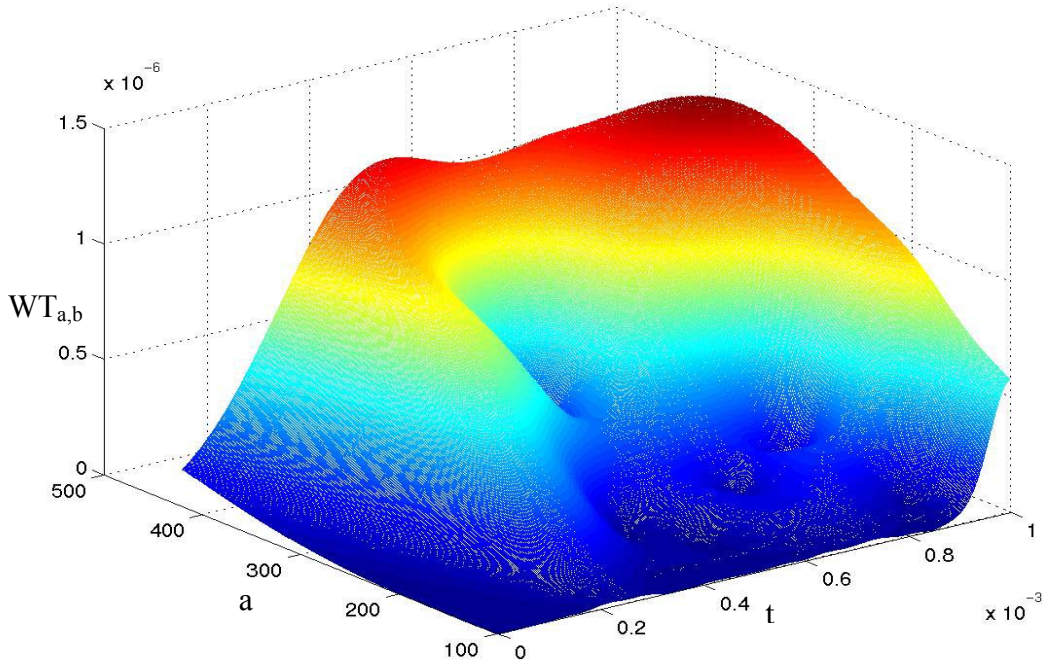

b) Wide band load

Figure 3-4 Wavelet Transform of signals recorded at sensor 1 in isotropic plate

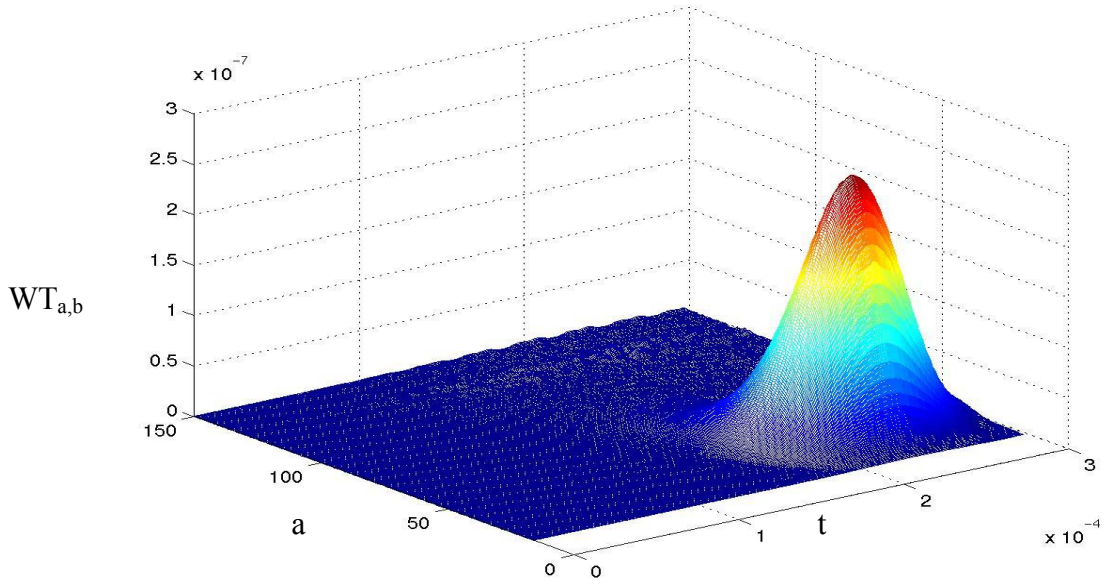

a) Narrow band load

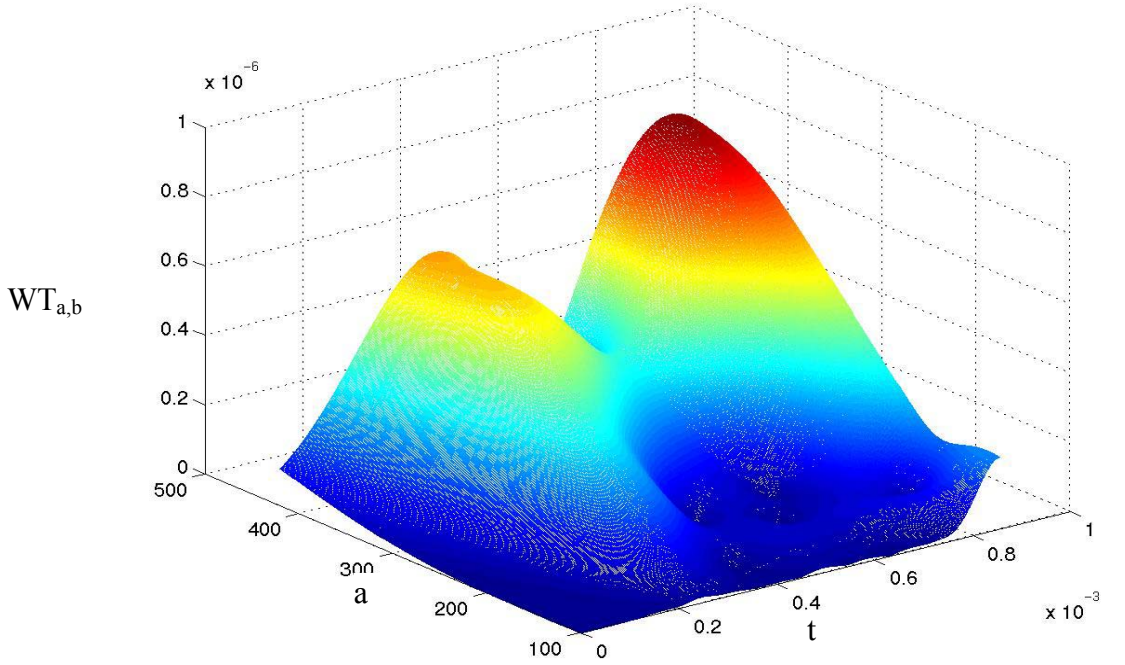

b) Wide band load

Figure 3-5 Wavelet transform of signal recorded at sensor 1 in composite plate 1

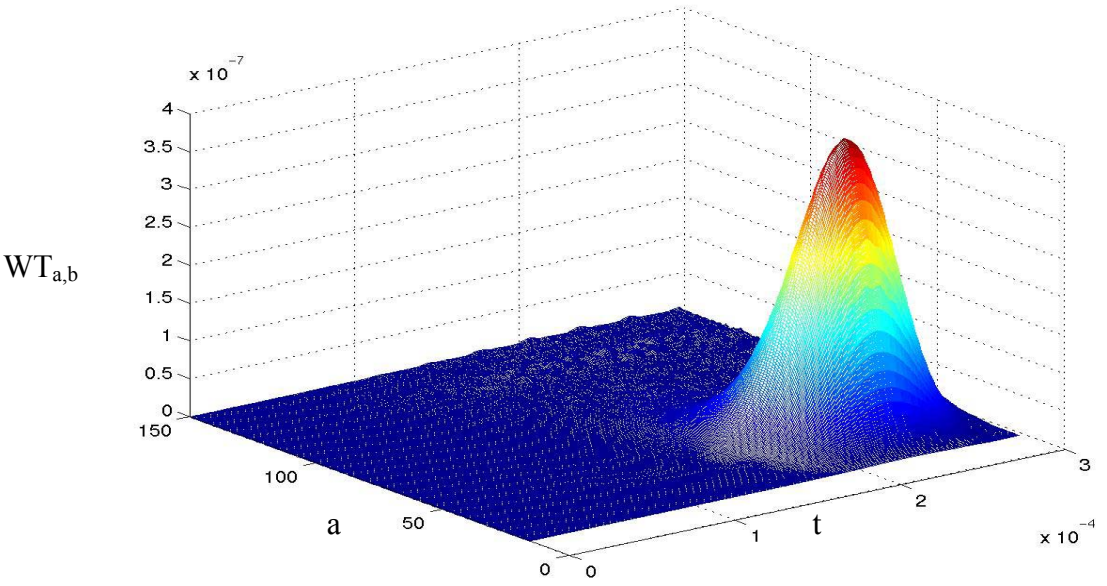

a) Narrow band load

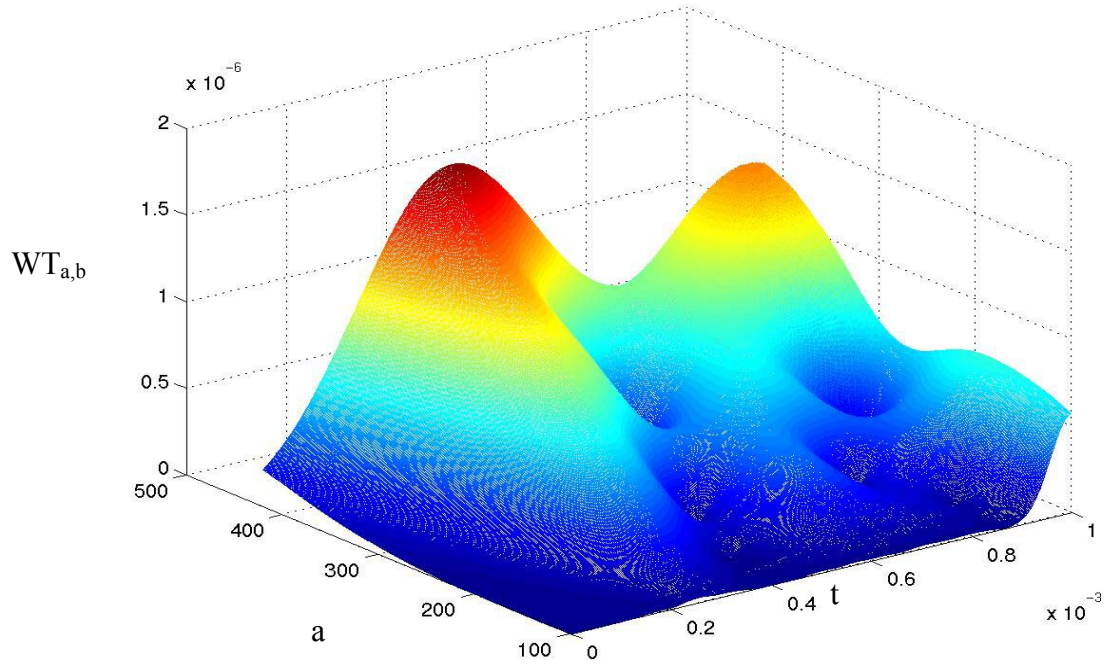

b) Wide band load

Figure 3-6 Wavelet transform of signal recorded at sensor 1 in composite plate 2

CHAPTER 4

ESTIMATION OF LOAD LOCATION

As we will explain later in this chapter, in order to solve the inverse problem and estimate the location of the point load we need to establish a set of nonlinear equations. Since we don't know the location of the point load, the directions of the scattering waves are unknown. Therefore, due to the variations of group velocities in different directions the group speeds are also unknown. So it is useful to study the wave propagation in plates and dispersion relations in order to find a relation between the direction of the propagating waves and velocities.

Presented here is some of the work which has been done with the purpose of either determining or verifying the dispersion relation in plate or beam structures. Plate theories are the most common methods to derive the dispersion relations. One approach to solve the wave scattering problem in plates is to represent the scattered field by wave function expansion, as reported by Abduljabbar et al. [1]. In order to represent the scattered wave field by the wave function expansion, displacement and stress eigenfunctions have to be established. Using elasticity equations, dispersion relation for a homogenous isotropic plate has been extensively studied by Mindlin [40]. Wave propagation in two-layer or three-layer (sandwich) isotropic plates have been analytically investigated by Yu [37], Jones and Lee and Chang [23]. Nayef and Chimenti [27] developed an analysis for wave propagation in a homogenous anisotropic

plate. Baylis [3] investigated analytical dispersion equations for two or three-layer transversely isotropic plates.

Karunasena et al. [21] studied the dispersion characteristics of guided waves in a cross-ply laminated plate. They employed both stiffness method and exact method to solve this problem, and used a Rayleigh-Ritz type of approximation for the through thickness variations of the displacements for this investigation. Jeong [18] analyzed the wave propagation in anisotropic laminates using a wavelet transform. Lin and Yuan [25] modeled the diagnostic transient waves in an integrated piezoelectric sensor/actuator plate. Park and Kim [29] evaluated the dispersive phase and group velocities using harmonic wavelet transform. Kishimoto et al. [22] presented an approach for investigation of the dispersive character of structural waves induced in a beam structure by applying the wavelet transform to the time-frequency analysis of waves. They could accurately identify the dispersion relation of the group velocity for a wide range of frequency. Aberg and Gudmundson [2] computed the dispersion relation for laminated composite plates with transverse matrix cracks. Gorman and Ziola [16] induced transverse matrix cracks in cross-ply laminate graphite-epoxy coupons by tensile loading in order to study the propagation of flexural and extensional waves. Presented here is the Mindlin's plate theory for composites to investigate the problem. Using this theory is particularly important in composites because of the effects of the shear deflection.

4.1 Dispersion Relation of Waves in Plates

The Mindlin plate theory is presented below. In the Mindlin's theory, shear and rotary inertia effects are taken into consideration [40]. Here a composite plate in the *x*-*y* plane without external loads is considered. The displacements are assumed to be:

$$u(x,y,z) = u^0(x,y,t) + z\psi_x(x,y,t)$$

$$v(x,y,z) = v^0(x,y,t) + z\psi_y(x,y,t) \tag{4.1}$$

$$w(x,y,z) = w^0(x,y,t)$$

where u,v,w are displacements of a point at (x,y,z) on the plate, u^0,v^0,w^0 defines the displacements of the mid plane and ψ_x, ψ_y are cross section rotations. The generalized in-plane stress resultants (N_x, N_y, and N_{xy}) and generalized bending moments (M_x, M_y, and M_{xy}) are defined as in classical plate theory in the vector form:

$$\boldsymbol{N} = \begin{Bmatrix} N_x \\ N_y \\ N_{xy} \end{Bmatrix} \qquad \boldsymbol{M} = \begin{Bmatrix} M_x \\ M_y \\ M_{xy} \end{Bmatrix} \tag{4.2}$$

Using Equation (4.1) in conjunction with the strain displacement relations, $\varepsilon_x = \frac{\partial u}{\partial x}, \varepsilon_y = \frac{\partial v}{\partial y}, \gamma_{xy} = \frac{\partial u}{\partial y} + \frac{\partial v}{\partial x}$, we obtain the following results

$$\varepsilon_x = \varepsilon_x^0 + z\kappa_x$$

$$\varepsilon_y = \varepsilon_y^0 + z\kappa_y \tag{4.3}$$

$$\gamma_{xy} = \gamma_{xy}^0 + z\kappa_{xy}$$

where $\varepsilon_x, \varepsilon_y, \gamma_{xy}$ are strain components and superscript 0 denotes the mid plane. The strains $(\varepsilon_x^0, \varepsilon_y^0, \text{and } \gamma_{xy}^0)$ and curvatures $(\kappa_x, \kappa_y, \text{and } \kappa_{xy})$ are defined as [2]:

$$\varepsilon_x^0 = \frac{\partial u^0}{\partial x} \qquad \varepsilon_y^0 = \frac{\partial v^0}{\partial y} \qquad \gamma_{xy}^0 = \frac{\partial u^0}{\partial y} + \frac{\partial v^0}{\partial x} \tag{4.4}$$

$$\kappa_x = \frac{\partial \psi_x}{\partial x} \qquad \kappa_y = \frac{\partial \psi_y}{\partial y} \qquad \kappa_{xy} = \frac{\partial \psi_x}{\partial y} + \frac{\partial \psi_y}{\partial x}$$

Introducing the following vector notations:

$$\boldsymbol{\varepsilon} = \begin{Bmatrix} \varepsilon_x \\ \varepsilon_y \\ \gamma_{xy} \end{Bmatrix} \; ; \quad \boldsymbol{\kappa} = \begin{Bmatrix} \kappa_x \\ \kappa_y \\ \kappa_{xy} \end{Bmatrix} \tag{4.5}$$

The stress-strain relationship in the laminate theory can be expressed as [19]:

$$\begin{Bmatrix} \boldsymbol{N} \\ \boldsymbol{M} \end{Bmatrix} = \begin{bmatrix} \boldsymbol{A} & \boldsymbol{B} \\ \boldsymbol{B} & \boldsymbol{D} \end{bmatrix} \begin{Bmatrix} \boldsymbol{\varepsilon} \\ \boldsymbol{\kappa} \end{Bmatrix} \tag{4.6}$$

where the submatrices **A** known as extensional stiffness, **B**, bending-extension stiffness, and **D** bending stiffness are defined as: [19]

$$\mathbf{A} = \begin{bmatrix} A_{11} & A_{12} & A_{16} \\ A_{12} & A_{22} & A_{26} \\ A_{16} & A_{26} & A_{66} \end{bmatrix} \quad \mathbf{B} = \begin{bmatrix} B_{11} & B_{12} & B_{16} \\ B_{12} & B_{22} & B_{26} \\ B_{16} & B_{26} & B_{66} \end{bmatrix} \quad \mathbf{D} = \begin{bmatrix} D_{11} & D_{12} & D_{16} \\ D_{12} & D_{22} & D_{26} \\ D_{16} & D_{26} & D_{66} \end{bmatrix} \tag{4.7}$$

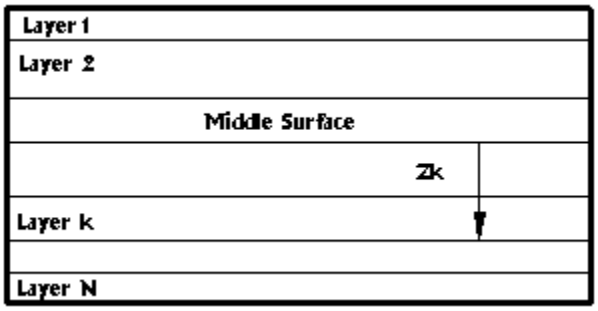

Figure 4-1 Schematic figure of cross section of a composite laminate

where,

$$A_{ij} = \sum_{1}^{N} (\overline{Q_{ij}})_k (Z_k - Z_{k-1})$$
$$B_{ij} = \frac{1}{2} \sum_{1}^{N} (\overline{Q_{ij}})_k (Z_k^2 - Z_{k-1}^2) \qquad (4.8)$$
$$D_{ij} = \frac{1}{3} \sum_{1}^{N} (\overline{Q_{ij}})_k (Z_k^3 - Z_{k-1}^3)$$

And $\overline{Q}_{ij}$ are the transformations of stiffness matrix Q_{ij} [19].

$$Q_{11} = \frac{E_1}{1 - \nu_{12}\nu_{21}} \qquad Q_{66} = G_{12}$$
$$Q_{12} = \frac{\nu_{12} E_2}{1 - \nu_{12}\nu_{21}} \qquad Q_{44} = G_{23} \qquad (4.9)$$
$$Q_{22} = \frac{E_2}{1 - \nu_{12}\nu_{21}} \qquad Q_{55} = G_{31}$$
$$Q_{45} = G_{23} - G_{31}$$

Applying the definition of the shear force resultants, we obtain an additional constitutive relation involving transverse shear. We introduce a parameter *k* in this constitutive relation for transverse shear and obtain [36]

$$\begin{Bmatrix} q_{yz} \\ q_{xz} \end{Bmatrix} = k \begin{bmatrix} A_{44} & A_{45} \\ A_{45} & A_{55} \end{bmatrix} \begin{Bmatrix} \gamma_{yz} \\ \gamma_{xz} \end{Bmatrix} \qquad (4.10)$$

where the interlaminar shear strains are given by the relationships

$$\gamma_{xz} = \frac{\partial u}{\partial z} + \frac{\partial w}{\partial x} = \psi_x + \frac{\partial w}{\partial x} \tag{4 .11}$$

$$\gamma_{yz} = \frac{\partial v}{\partial z} + \frac{\partial w}{\partial y} = \psi_y + \frac{\partial w}{\partial y}$$

The shear-correction factor (k) is chosen to be 5/6 following Whitney [36]. Using the governing equations of motion in terms of stress and moment resultants, we have [19]:

$$\frac{\partial N_x}{\partial x} + \frac{\partial N_{xy}}{\partial y} = \rho h \frac{\partial^2 u^0}{\partial t^2} \tag{4.12}$$

$$\frac{\partial N_{xy}}{\partial x} + \frac{\partial N_y}{\partial y} = \rho h \frac{\partial^2 v^0}{\partial t^2} \tag{4.13}$$

$$\frac{\partial M_x}{\partial x} + \frac{\partial M_{xy}}{\partial y} - q_{xz} = I \frac{\partial^2 \psi_x}{\partial t^2} \tag{4.14}$$

$$\frac{\partial M_{xy}}{\partial x} + \frac{\partial M_y}{\partial y} - q_{yz} = I \frac{\partial^2 \psi_y}{\partial t^2} \tag{4.15}$$

$$\frac{\partial q_{xz}}{\partial x} + \frac{\partial q_{yz}}{\partial y} = \rho h \frac{\partial^2 w}{\partial t^2} \tag{4.16}$$

where I is the mass moment of inertia. Using the equations of motion stated above, and taking Equations (4.4) to (4.7) into account, we have,

$$A_{11}\frac{\partial^2 u^0}{\partial x^2}+2A_{16}\frac{\partial^2 u^0}{\partial x\partial y}+A_{66}\frac{\partial^2 u^0}{\partial y^2}+A_{16}\frac{\partial^2 v^0}{\partial x^2}+(A_{12}+A_{66})\frac{\partial^2 v^0}{\partial x\partial y}+A_{26}\frac{\partial^2 v^0}{\partial y^2}$$
$$+B_{11}\frac{\partial^2 \psi_x}{\partial x^2}+2B_{16}\frac{\partial^2 \psi_x}{\partial x\partial y}+B_{66}\frac{\partial^2 \psi_x}{\partial y^2}+B_{16}\frac{\partial^2 \psi_y}{\partial x^2}+(B_{12}+B_{66})\frac{\partial^2 \psi_y}{\partial x\partial y}+B_{26}\frac{\partial^2 \psi_y}{\partial y^2}$$
$$=\rho h\frac{\partial^2 u^0}{\partial t^2}$$

$$A_{16}\frac{\partial^2 u^0}{\partial x^2}+(A_{12}+A_{66})\frac{\partial^2 u^0}{\partial x\partial y}+A_{26}\frac{\partial^2 u^0}{\partial y^2}+A_{66}\frac{\partial^2 v^0}{\partial x^2}+2A_{26}\frac{\partial^2 v^0}{\partial x\partial y}+A_{22}\frac{\partial^2 v^0}{\partial y^2}+$$
$$B_{16}\frac{\partial^2 \psi_x}{\partial x^2}+(B_{12}+B_{66})\frac{\partial^2 \psi_x}{\partial x\partial y}+B_{26}\frac{\partial^2 \psi_x}{\partial y^2}+B_{66}\frac{\partial^2 \psi_y}{\partial x^2}+2B_{26}\frac{\partial^2 \psi_y}{\partial x\partial y}+B_{22}\frac{\partial^2 \psi_y}{\partial y^2}=$$
$$\rho h\frac{\partial^2 v^0}{\partial t^2}$$

(4.18)

$$B_{11}\frac{\partial^2 u^0}{\partial x^2}+2B_{16}\frac{\partial^2 u^0}{\partial x\partial y}+B_{66}\frac{\partial^2 u^0}{\partial y^2}+B_{16}\frac{\partial^2 v^0}{\partial x^2}+(B_{12}+B_{66})\frac{\partial^2 v^0}{\partial x\partial y}+B_{26}\frac{\partial^2 v^0}{\partial y^2}+$$
$$D_{11}\frac{\partial^2 \psi_x}{\partial x^2}+2D_{16}\frac{\partial^2 \psi_x}{\partial x\partial y}+D_{66}\frac{\partial^2 \psi_x}{\partial y^2}+D_{16}\frac{\partial^2 \psi_y}{\partial x^2}+(D_{12}+D_{66})\frac{\partial^2 \psi_y}{\partial x\partial y}+D_{26}\frac{\partial^2 \psi_y}{\partial y^2}$$
$$-k[A_{55}(\psi_x+\frac{\partial w}{\partial x})+A_{45}(\psi_y+\frac{\partial w}{\partial y})]=I\frac{\partial^2 \psi_x}{\partial t^2}$$

(4.19)

$$B_{16}\frac{\partial^2 u^0}{\partial x^2}+(B_{12}+B_{66})\frac{\partial^2 u^0}{\partial x\partial y}+B_{26}\frac{\partial^2 u^0}{\partial y^2}+B_{66}\frac{\partial^2 v^0}{\partial x^2}+2B_{26}\frac{\partial^2 v^0}{\partial x\partial y}+B_{22}\frac{\partial^2 v^0}{\partial y^2}+$$
$$D_{16}\frac{\partial^2 \psi_x}{\partial x^2}+(D_{12}+D_{66})\frac{\partial^2 \psi_x}{\partial x\partial y}+D_{26}\frac{\partial^2 \psi_x}{\partial y^2}+D_{66}\frac{\partial^2 \psi_y}{\partial x^2}+2D_{26}\frac{\partial^2 \psi_y}{\partial x\partial y}+D_{22}\frac{\partial^2 \psi_y}{\partial y^2}$$
$$-k[A_{45}(\psi_x+\frac{\partial w}{\partial x})+A_{44}(\psi_y+\frac{\partial w}{\partial y})]=I\frac{\partial^2 \psi_y}{\partial t^2}$$

(4.20)

$$k\left(A_{55}(\frac{\partial \psi_x}{\partial x}+\frac{\partial^2 w}{\partial x^2})+A_{45}(\frac{\partial \psi_x}{\partial y}+\frac{\partial \psi_y}{\partial x}+2\frac{\partial^2 w}{\partial x \partial y})+A_{44}(\frac{\partial \psi_y}{\partial y}+\frac{\partial^2 w}{\partial y^2}) \right)=\rho h \frac{\partial^2 w}{\partial t^2}$$

(4.21)

In the case of harmonic wave propagation, it is further assumed that the displacement functions take the form:

$$(u^0, v^0, w^0, \psi_x, \psi_y)=(U, V, W, \Psi_x, \Psi_y)e^{i(k_x x+k_y y-\omega t)} \qquad (4.22)$$

where the capital letters are complex-valued constants, k_x and k_y are the x and y-components of the wave vector, respectively, and ω is the circular frequency. Substituting equation (4.22) into the equations of motion, i.e., Equations (4.17) through (4.21) for the laminate yields the following generalized eigenvalue problem [2]:

$$\left(\begin{bmatrix} K_{11} & K_{12} & K_{13} & K_{14} & K_{15} \\ K_{12} & K_{22} & K_{23} & K_{24} & K_{25} \\ K_{13} & K_{23} & K_{33} & K_{34} & K_{35} \\ K_{14} & K_{24} & -K_{34} & K_{44} & K_{45} \\ K_{15} & K_{25} & -K_{35} & K_{45} & K_{55} \end{bmatrix} - \omega^2 \begin{bmatrix} \rho h & 0 & 0 & 0 & 0 \\ 0 & \rho h & 0 & 0 & 0 \\ 0 & 0 & \rho h & 0 & 0 \\ 0 & 0 & 0 & \frac{\rho h^3}{12} & 0 \\ 0 & 0 & 0 & 0 & \frac{\rho h^3}{12} \end{bmatrix} \right) \begin{Bmatrix} U \\ V \\ W \\ \psi_x \\ \psi_y \end{Bmatrix} = \begin{Bmatrix} 0 \\ 0 \\ 0 \\ 0 \\ 0 \end{Bmatrix}$$

(4.23)

where ρ is the density, which is assumed to be the same in all plies, and h is the thickness of the laminate. The $K_{ij}s$, which depend on the wave vector and laminate stiffness elements, are given by

$$K_{11} = A_{11}k_x^2 + 2A_{16}k_x k_y + A_{66}k_y^2,$$

$$K_{12} = A_{16}k_x^2 + (A_{12} + A_{66})k_x k_y + A_{26}k_{y,}^2$$

$$K_{13} = 0, \qquad K_{14} = B_{11}k_x^2 + 2B_{16}k_x k_y + B_{66}k_y^2,$$

$$K_{15} = B_{16}k_x^2 + (B_{12} + B_{66})k_x k_y + B_{26}k_y^2, \tag{4.24}$$

$$K_{22} = A_{66}k_x^2 + 2A_{26}k_x k_y + A_{22}k_y^2, \qquad K_{23} = 0,$$

$$K_{24} = B_{16}k_x^2 + (B_{66} + B_{12})k_x k_y + B_{26}k_y^2,$$

$$K_{25} = B_{66}k_x^2 + 2B_{26}k_x k_y + B_{22}k_y^2,$$

$$K_{33} = A_{55}kk_x^2 + 2A_{45}kk_x k_y + A_{44}kk_y^2,$$

$$K_{34} = -i(A_{55}kk_x + A_{45}kk_y),$$

$$K_{35} = -i(A_{44}kk_y + A_{45}kk_x),$$

$$K_{44} = D_{11}k_x^2 + 2D_{16}k_x k_y + D_{66}k_y^2 + A_{55}k,$$

$$K_{45} = D_{16}k_x^2 + (D_{12} + D_{66})k_x k_y + D_{26}k_y^2 + A_{45}k,$$

$$K_{55} = D_{66}k_x^2 + 2D_{26}k_x k_y + D_{22}k_y^2 + A_{44}k,$$

For given wave vector components, k_x and k_y, the generalized eigen value problem of Equation (4.23) gives five eigen frequencies which are real ω since K is a Hermitian matrix [2]. Note that the elements K_{34} and K_{35} are pure imaginary.

Once ω as a function of k_x and k_y is known, the phase and group velocities are determined using the relations

$$c_p = \omega / k \ ; \qquad c_g = d\omega / dk \tag{4.25}$$

For the sake of convenience the dimensionless phase velocity and circular frequency are defined as:

$$\hat{c}_p = \frac{\omega}{k}\sqrt{\frac{\rho}{E_1}}$$

$$\hat{\omega} = \omega\sqrt{\frac{\rho h^2}{E_1}} \tag{4.26}$$

The dimensionless phase velocities along different angles are plotted in Figures 4-3 to 4-5. The first three modes shown in the plots are acoustic modes which can also propagate in lower frequencies. The lowest one corresponds to the flexural mode, the second is in the plane shear and the third one is the extensional mode The frequency from which the other two modes, known as optical modes, start to propagate is called the cut-off frequency and these modes are related to ψ_x and ψ_x, which are rotations of the cross section.

In this study we are interested in the first acoustic mode which is the transverse deflection W and its group and phase velocities are plotted in Figures 4-6 to 4-9 for the composite plates. For composite plate 1 we have three axes of symmetry around $\theta = 0^0, 45^0, 90^0$ and for composite plate 2 we have two axes of symmetry around $\theta = 0^0, 90^0$ and this fact is clearly shown in these figures. The fiber orientation of composite plate 2 is shown in Figure 4-2. Note that the wave vector components satisfy the equation $\theta = \arctan(k_y / k_x)$, where θ is the angle

of wave propagation. Figures 4-10 to 4-11 show the group velocities versus θ for some frequencies in each of the composite plates. It can also be seen in these Figures that the group velocities are higher for higher frequencies.

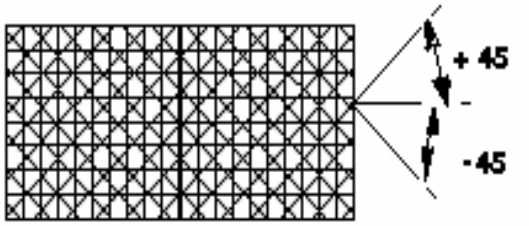

Figure4-2 Schematic view of the fiber orientations of composite plate 2 [+45/0/-45]

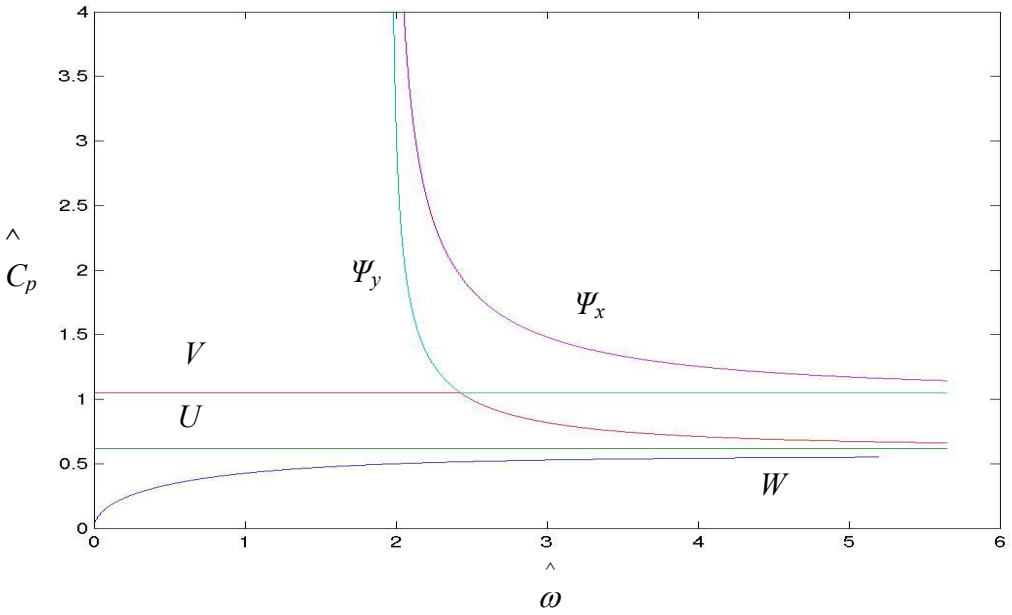

Figure 4-3 Dimensionless C_p versus ω in isotropic plate

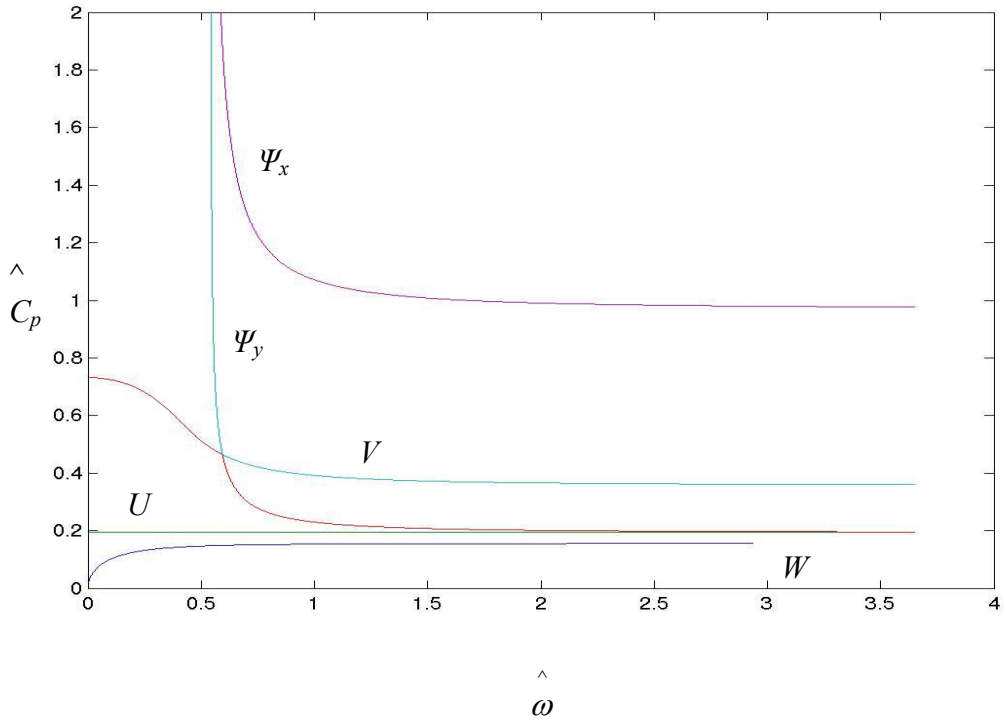

Figure 4-4 Dimensionless C_p versus ω for θ=0 in composite plate 1

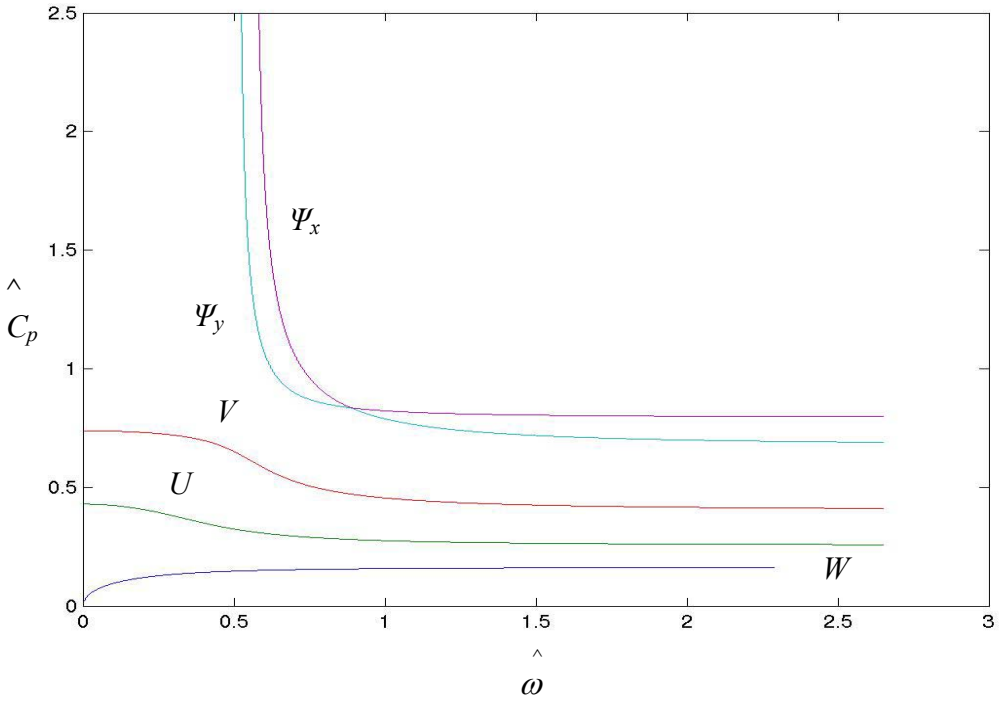

Figure 4-5 Dimensionless C_p versus ω for θ=0 in composite plate 2

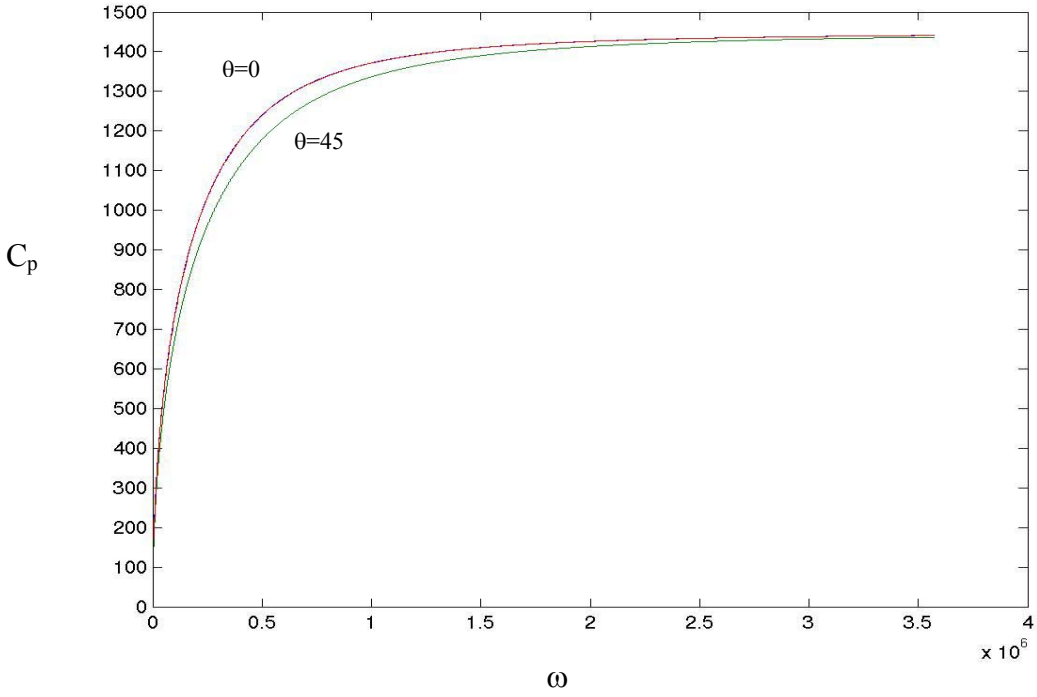

Figure 4-6 Phase velocity of the first acoustic mode in composite plate 1

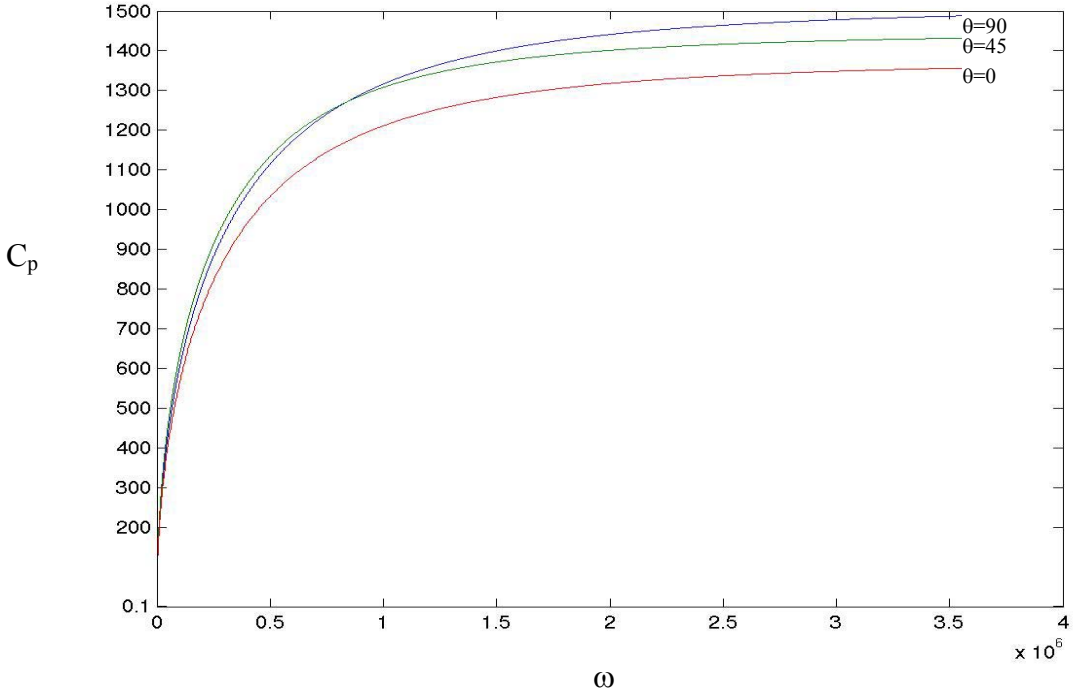

Figure 4-7 Phase velocity of the first acoustic mode in composite plate 2

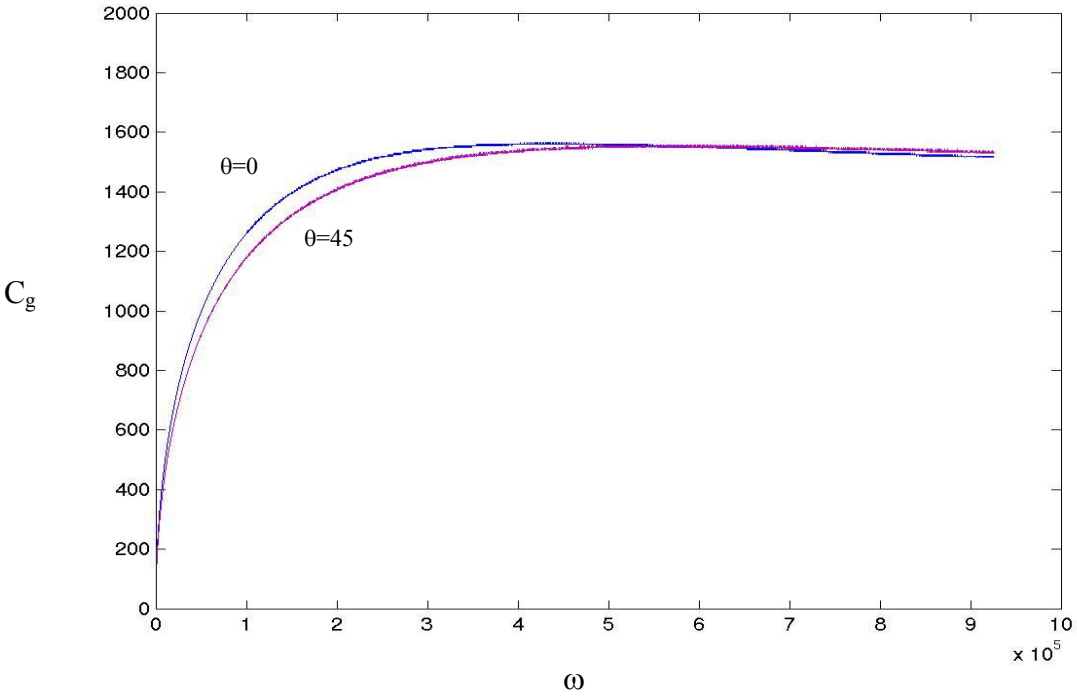

Figure 4-8 Group velocity of the first acoustic mode in composite plate 1

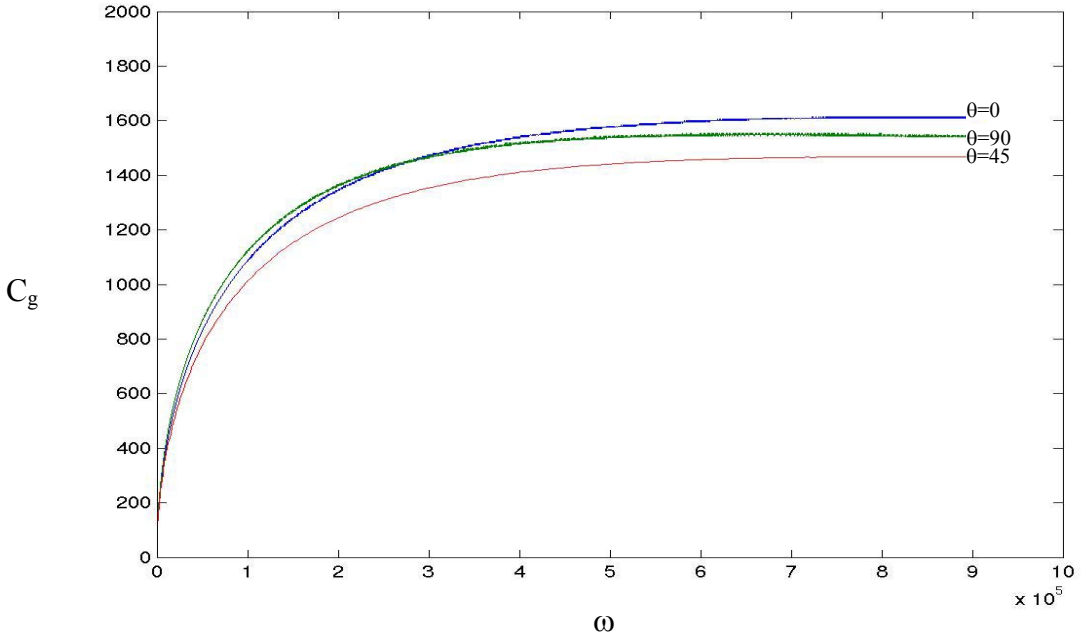

Figure4-9 Group velocity of the first acoustic mode in composite plate 2

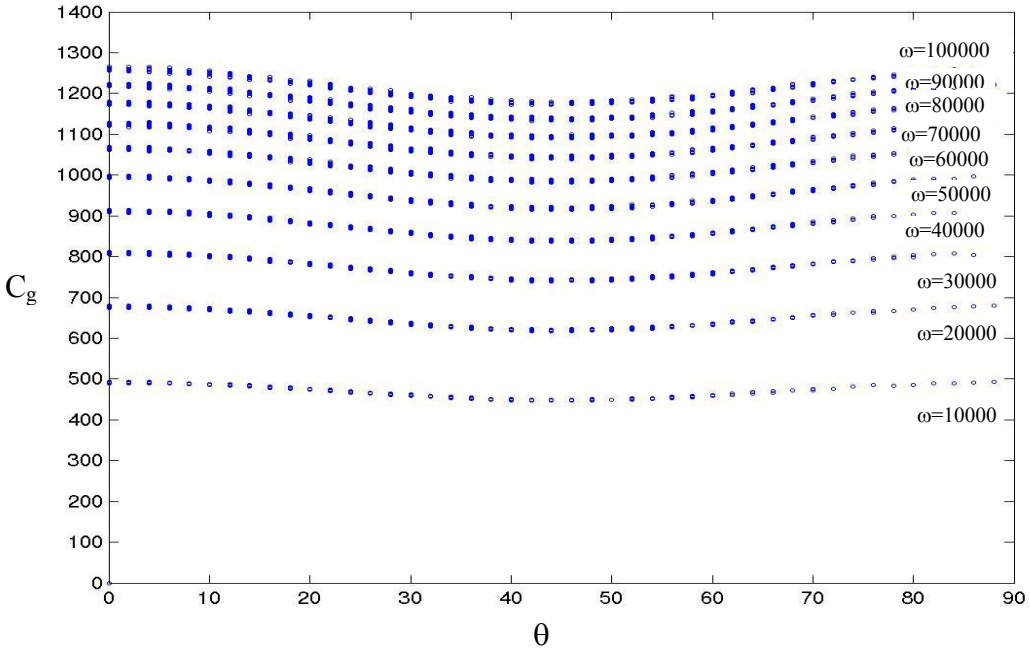

Figure4-10 Group velocities for some frequencies versus θ in composite plate 1

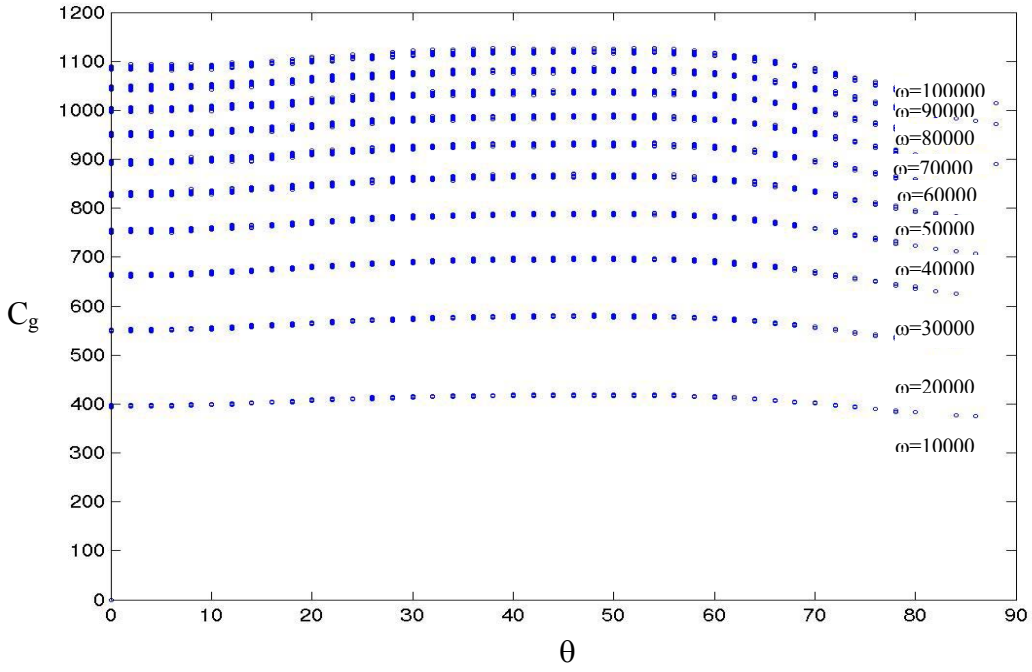

Figure 4-11 Group velocities for some frequencies versus θ in composite plate 2

4.2 Identifying the Impact Load Location

Mathematically, the wavelet transform defined by Equation (3.1) can be understood as the inner product of the recorded signal and the wavelet function in a functional space, which measures the similarity between the shape of the signal and the wavelet function. When parameters a and b are values that the shape of the signal and the wavelet function match the best, we get the maximum value for the wavelet coefficient. As mentioned before, the time shift which maximizes the inner product of the wavelet function for scale a and the signal recorded at each sensor is the arrival time related to the frequency associated with that scale by $\omega = \frac{\omega_0}{a\Delta t}$ or $f = \frac{f_0}{a\Delta t}$. In this part of the chapter we use the arrival times for dominant frequency contents of a signal, given by the wavelet approach presented in the previous chapter. A system of nonlinear equations can be formulated to estimate the location of the applied load.

4.2.1 Isotropic Plate

Once the signals are recorded and their frequency contents are found, one can relate a range of frequencies in the signal to a range of scale. Then a continuous wavelet transformation is applied to find the peak values for dominant frequency contents of the signal. Note that only the first peak is related to the arrival time for the shortest path of the propagating waves. Once the arrival times, are known,

the location of the impact can be found by the following set of nonlinear equations for isotropic plate.

$$l_i = \sqrt{((x - x_p)^2 + (y - y_p)^2}$$
$$t_i(\omega) = \frac{l_i}{cg(\omega)} \qquad (4.27)$$
$$(i = 1,2,3)$$

where l_i is the distance between the sensor i and the impact location, $t_i(\omega)$ is the arrival time of frequency components ω to sensor i, and x_p, y_p are the coordinates of the impact location. The system of six Equations in (4.27) can be solved for six unknowns involved and the location of the impact can be found for a range of frequency contents in the signal. As mentioned before the complication of this study is for the composite plates due to the variations of the group velocity in different directions. So for the simple case of isotropic plate, there is no necessity for taking the group velocities of dispersion relation, however, this can be a method for the purpose of verifying the dispersion relation as done previously by Gaul and Hurlebaus [14].

4.2.2 Composite Plate

For the composite plate the solution is more complicated for the reason stated before, so we have more than one C_g as unknown. In order to overcome this complexity, the velocities from dispersion relations are used for the composite case. Such variations for the phase and group velocities versus θ for different frequencies are plotted in Figures 4-10 and 4-11. So we have another system of nonlinear equations to solve for unknowns θ_i shown on Figure 4-12. Without loss of generality the point load has been shown inside the triangular sensor location. The same equations will apply for the case of impact load out of triangular with taking the sign convention of angles in to consideration. By finding the arrival times to each sensor S_i for frequency *f*, one can find:

$$\Delta t_{12}(f) = t_1(f) - t_2(f) = \frac{l_1}{C_{g_1}(f)} - \frac{l_2}{C_{g_2}(f)}$$
$$\Delta t_{23}(f) = t_2(f) - t_3(f) = \frac{l_2}{C_{g_2}(f)} - \frac{l_3}{C_{g_3}(f)} \qquad (4.28)$$

where,

l_i = distance between sensor i and the impact location

Δt_{ij} = arrival time difference between sensors i and j

t_i = arrival time to sensor i

Cg_i = group velocity in the θ_i direction.

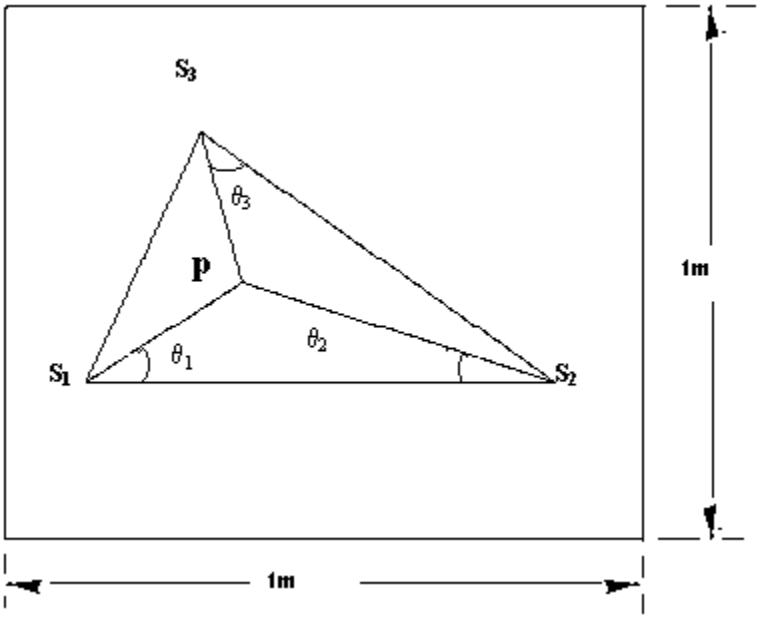

Figure 4-12 Schematic figure of the plate with location of sensors and source P

Also we know:

$$\begin{aligned} l_1 \sin(\theta_1) &= l_2 \sin(\theta_2) \\ l_1 \cos(\theta_1) + l_2 \cos(\theta_2) &= S_1 S_2 \end{aligned} \tag{4.29}$$

and from there we get:

$$\begin{aligned} l_1 &= \frac{S_1 S_2}{\sin(\theta_1)\left(\cot g(\theta_1) + \cot g(\theta_2)\right)} \\ l_2 &= \frac{S_1 S_2}{\sin(\theta_2)\left(\cot g(\theta_1) + \cot g(\theta_2)\right)} \end{aligned} \tag{4.30}$$

where,

$S_i S_j$ = distance between sensors i and j

By writing the same equations for $l_2, l_3, \theta_2, \theta_3$ we have:

$$l_2 = \frac{S_2 S_3}{\sin(\hat{S_2} - \theta_2)\left(\cot g(\theta_3) + \cot g(\hat{S_2} - \theta_2)\right)}$$

$$l_3 = \frac{S_2 S_3}{\sin(\theta_3)\left(\cot g(\theta_3) + \cot g(\hat{S_2} - \theta_2)\right)}$$

(4.31)

Substituting Equations(4.30) and (4.31) into Equation (4.28),

$$\frac{1}{\cot g(\theta_1) + \cot g(\theta_2)}\left(\frac{1}{\sin(\theta_1).cg_1} - \frac{1}{\sin(\theta_2).cg_2}\right) - \frac{\Delta t_{12}}{S_1 S_2} = 0$$

$$\frac{1}{\cot g(\theta_3) + \cot g(\hat{S_2} - \theta_2)}\left(\frac{1}{\sin(\hat{S_2} - \theta_2).cg_2} - \frac{1}{\sin(\theta_3).cg_3}\right) - \frac{\Delta t_{23}}{S_2 S_3} = 0$$

(4.32)

where,

$$\cot g(\theta_3) = \frac{S_2 S_3 . \sin(\theta_2)\left(\cot g(\theta_1) + \cot g(\theta_2)\right)}{S_1 S_2 \sin(\hat{S_2} - \theta_2)} - \cot g(\hat{S_2} - \theta_2)$$

(4.33)

By solving the above set of nonlinear Equations (4.32) and (4.33), θ_1 and θ_2 can be found, from which x_p and y_p, i.e., the coordinates of load location can be determined for each frequency f.

4.3 Numerical Results

To estimate the location of the load, the numerically simulated signals by ANSYS

are used. The load is applied at a specific location and the signals are recorded at various points of the plate. The set of nonlinear equations described in section 4.2 are employed to determine the load location.

4.3.1 Isotropic Plate

The results for the isotropic plate are shown in Figure 4-13. For both narrow band and wide band loads the impact location estimated by the wavelet approach is in good agreement with the location where the load is actually applied in the simulation, i.e., (0.5, 0.7) in meters. Note that he results are consistently good for the range of dominant frequency contents in the signal. The maximum percentage of error is 1.1%.

4.3.2 Composite Plates

The results for the composite plate are shown in Table 4-1. Tables 3-1 and 3-2 in Chapter 3 show the arrival times for different frequency contents to sensors in each case. As we expect from the dispersion relation the arrival times become smaller as the frequency increases due to the increase of the group velocities. Again, the results are in good agreement with the actual location of the applied load in the case of anisotropic plate. Note that the error in estimation of the coordinates of the load location is less than 1.2% for all different types of loading and both isotropic and anisotropic plates. The solid lines show the reference line and the lines with circles are the calculated ones.

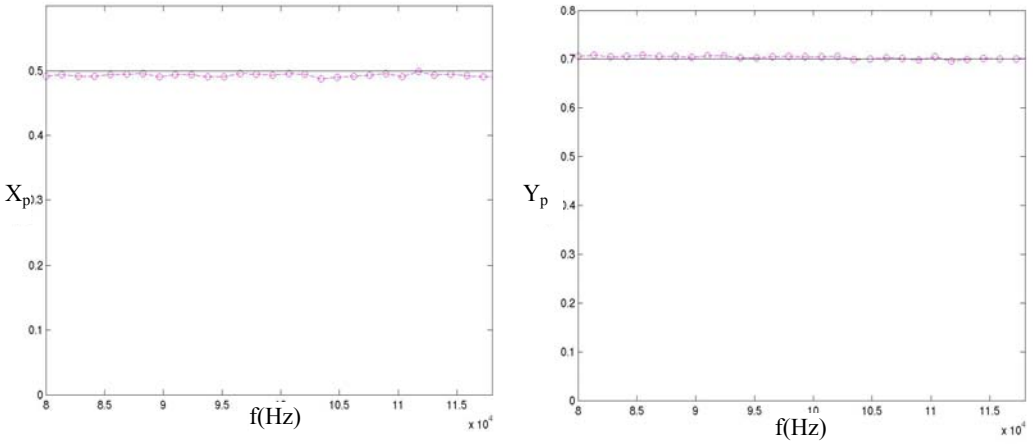

a) narrow band five peak load

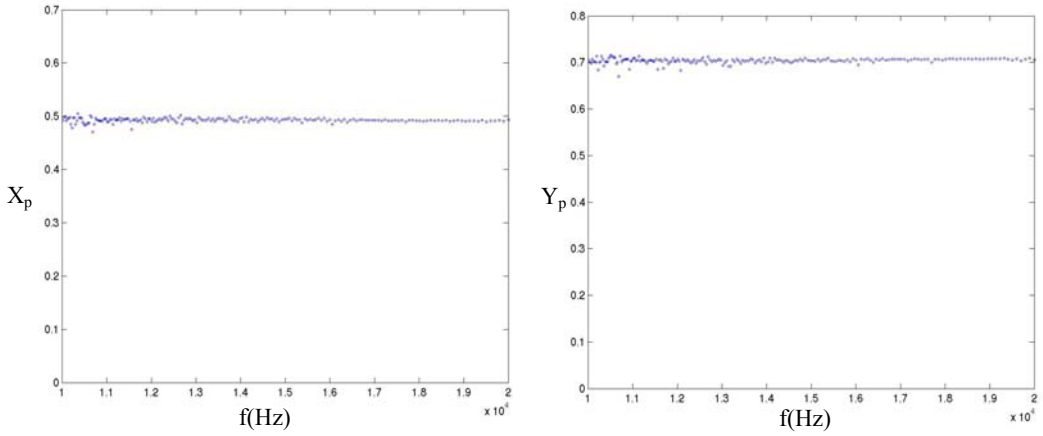

b) wide band triangular load

Figure 4-13 Estimated coordinates of the impact location for isotropic plate

Table 4-1 Estimated location of the applied load by wavelet approach for composite plates (m)

Loading / Plate		Wide Band Load					Narrow Band Load
		9.5 (KHz)	15.9 (KHz)	23.8 (KHz)	31.8 (KHz)	39.8 (KHz)	100.2 (KHz)
Composite 1	x	.4978	.4938	.5025	.4981	.4978	.5025
	y	.6964	.7059	.7002	.7030	.6964	.7002
Composite 2	x	.4938	.5025	.5025	.4981	.5025	.5025
	y	.7059	.7002	.7002	.7030	.7002	.7002

4.4 Robustness of the Method for Noised Signal

In reality the measured signals from the sensors are different from the numerical simulations, and this is because the data is often contaminated by measurement noises. In this section the noise effects on the results are addressed. So we incorporate noise in the measured signals as follow:

$$y(t) = x(t) + n(t) \tag{4.34}$$

where x is the original signal, y is the noised signal and $n(t)$ is the measurement noise which can be expressed as:

$$n(t) = rms \times s \times r(t) \tag{4.35}$$

and rms is the root mean square of the signal x, $r(t)$ is a function which generates arrays of random numbers whose elements are normally distributed with mean 0, variance $\sigma^2 = 1$, and standard deviation of $\sigma = 1$, and s is referred to as noise level which is inverse proportional to the so called SNR (signal to noise ratio).

After adding certain percentage of white noise to the system, and denoising the signal by a common method of moving average, we apply the same method to determine the impact location. The results for the same sensors S_1, S_2, S_3 for two different noise levels of 2% and 5% were tested and they are shown in Tables 4-2 to 4-4. The maximum error of 1.4% for different frequency contents in the signal shows the robustness of this method. The results were also tested for noise 7%. Such results are presented in Appendix B. A sample signal measured from one of the sensors in composite plate 2 with a noise level of 7% is shown in Figure 4-14. The white trace line in the middle of the plotted signal shows the signal after denoising.

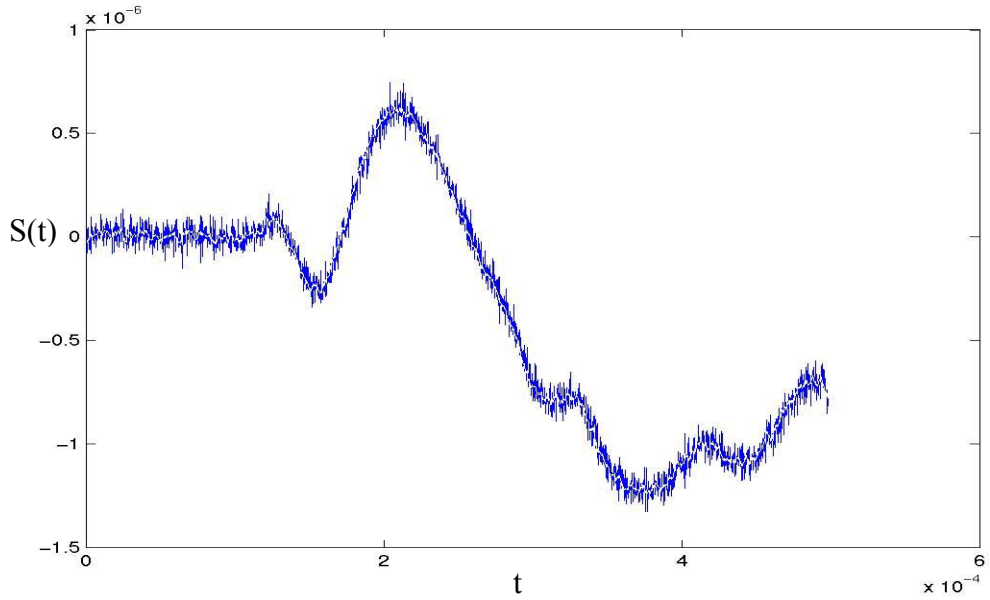

Figure 4-14 Signal measured from one of the sensors in composite plate 2 contaminated with noise level 7%
(white trace line in the middle is the signal after removing the noise)

Table 4-2 Arrival times for different frequency Contents to sensors for composite plate 1 for the noised signals (10^{-4}sec.)

Noise	Noise level 2%-SNR 50			Noise level 5%-SNR 20		
Freq. / Sensor	23.8 (KHz)	31.8 (KHz)	39.8 (KHz)	23.8 (KHz)	31.8 (KHz)	39.8 (KHz)
S_1	2.74	2.59	2.49	2.65	2.455	2.73
S_2	3.025	2.97	2.83	3.015	2.805	2.995
S_3	2.435	2.435	2.2	2.31	2.275	2.455

Table 4-3 Arrival times for different frequency Contents to sensors for composite plate 2 the noised signals (10^{-4}sec.)

Noise	Noise level 2%-SNR 50			Noise level 5%-SNR 20		
Freq. / Sensor	23.8 (KHz)	31.8 (KHz)	39.8 (KHz)	23.8 (KHz)	31.8 (KHz)	39.8 (KHz)
S_1	2.725	2.485	2.81	2.725	2.575	2.82
S_2	3.05	2.85	3.165	3.045	2.84	3.21
S_3	2.45	2.33	2.57	2.405	2.395	2.545

Table 4-4 Estimated load location for signals contaminated with noise (m)

Noise / Plate		Noise level 2% -SNR 50			Noise level 5%-SNR 20		
		23.8 (KHz)	31.8 (KHz)	39.8 (KHz)	23.8 (KHz)	31.8 (KHz)	39.8 (KHz)
Composite1	x	0.5072	0.4974	0.4980	0.4985	0.4974	0.5072
	y	0.7040	0.6898	0.7030	0.7099	0.6898	0.7040
Composite2	x	0.5025	0.4978	0.5025	0.5028	0.5070	0.4981
	y	0.7002	0.6964	0.7002	0.7070	0.6973	0.7030

CHAPTER 5

CONCLUSION AND DISCUSSION

This research presents a general approach for an inverse problem to locate a sudden structural damage in isotropic and composite plates. The sudden damage is modeled as an impulse load and response data are collected at a set of sensor locations. The responses were then analyzed by a wavelet transform and the map of wavelet coefficients of each signal was utilized to estimate the arrival times of flexural waves by locating the peak value of wavelet coefficients. Then using a set of nonlinear equations the location of the applied load was determined.

The challenging part of this problem is the variations of the group velocities in different directions. Therefore, the calculated group velocities from dispersion relations of wave propagation based on the Mindlin's plate theory are employed to solve the problem.

The approach was validated for an isotropic plate and an anisotropic composite plate subjected to both narrow band and wideband loading where response data was generated by numerical simulation using the commercial finite element ANSYS codes. The estimated locations for both plates have shown excellent agreement with the actual locations of the impact loads applied. This shows that the wavelet transform can be effectively used to estimate the arrival times of scattering waves and hence the load location. In order to show the robustness of this method the effect of noise was also investigated and the results

agree well with the impact location. The error for all different types of plates, loading and SNR 50, 20 and 15 is less than 1.4%.

As we see in the tables presented in Chapter 4, the arrival times get smaller for the higher frequencies and this is expected due to the fact that group velocities are bigger for larger frequencies of the first acoustic mode.

The presented approach can be extended to determine the time history of the loading by different methods such as Neural Network. The force time history can be interpreted as severity of the damage in that case. One of the weaknesses of this method is when we get reflections from the boundaries, as those reflections mix with the scattering waves coming from the source the wavelet method fails to locate the peak values accurately. So it is essential to use the sensors far enough from the boundary to get a better estimation of the load location which is interpreted as the sudden damage. Also this method is only able to locate the initiation of the damage and can't predict the location of the developing cracks. In that case we basically have more than one wave source happening at different times, and trying to locate the peak values for a combination of sensors will be very complicated.

REFERENCES

1. Abduljabbar, Z., Datta, S.K., Shah, A. H., (1983). Diffraction of Horizontally Polarized Shear Waves by Normal Edge Cracks in a Plate. Journal of Applied Physics, 54 (2), 461-472.

2. Aberg, M., Gudmundson, P., (1998). Dispersion of Waves in Composite Laminates With Transverse Matrix Cracks, Finite Element and Plate Theory Computation. ASME Journal of Applied Mechanics, 65, 588-595.

3. Baylis, E.R., Green, W.A., (1986). Flexural Waves in Fiber Reinforced Laminated Plates. Journal of Sound and Vibrations, 110(1), 1-26.

4. Cruz, J.D. , Crisp, J.D., Ryall, T.G., (1992). Determining a Force Acting On a Plate–An Inverse Problem. AIAA Journal 29(3) 464-470.

5. Cruz, J.D., Crisp, D.C., (1992). On the Identification of a Harmonic Force on a Viscoelastic Plate from Response Data. Journal of applied Mechanics, 59, 722-728.

6. Choi, K., Chang, F.K., (1996). Identification Of Impact Force And Location Using Distributed Sensors. AIAA Journal 34(1), 136-141.

7. Doyle, J.F., (1987). An Experimental Method for Determining the Location and the time of Initiation of an Unknown Dispersing Pulse. Experimental Mechanics 27(3), 229-233.

8. Doyle, J.F., (1993). Force Identification From Dynamic Responses Of a Bimaterial Beam. Experimental Mechanics 33, 64-69.

9. Doyle, J.F., (1996). Impact Force Identification from Wave Propagation Responses. International Journal of Impact Engineering, 18(1), 65-77.

10. Doyle, J.F., (1997). Wave Propagation in Structures, Springer-Verlag Inc. NY.

11. Doyle, J.F., (1984). Further Developments in Determining the Dynamic Contact Law. Experimental Mechanics 24, 265-270.

12. Doyle, J.F., (1987). Determining the Contact Force During the Transverse Impact of Plates. Experimental Mechanics 27, 68-72.

13. Strang, G., (1997). Wavelets and Filter Banks, Wellesley-Cambridge Press.

14. Gaul, L., Hurlebaus, S., (2000). Wavelet-Transform to Identify the Location and Force-Time-History of Transient Load in a plate. Proceedings of the Second International Workshop on Structural Health Monitoring, Stanford university, Stanford, CA., 851-860.

15. Gaul, L., Hurlebaus, S., (1997). Identification of The Impact Location on a Plate Using Wavelets. Mechanical Systems and Signal Processing 12(6), 783-795.

16. Gorman, M.R., Ziola , S.M., (1991). Plate Waves Produced by Transverse Matrix Cracking. Ultrasonics 29, 245-251.

17. Inoue, H., Kishimoto, K., Shibuya, T., (1996). Experimental Wavelet Analysis of Flexural Waves in Beams. JSME International Journal 36(3) 212-217.

18. Jeong, H. (2001). Analysis of Plate Wave Propagation in Anisotrpic Laminates Using Wavelet Transform. NDT & International 34, 185-190.

19. Jones, R.M., (1991). Mechanics of Composite Materials. Taylor & Francis, Inc., Philadelphia, PA.

20. Kapania, R.K., Raciti, S., (1989). Recent Advances in Analysis of Laminated Beams and Plates, part 2 Vibrations and Wave Propagation. AIAA Journal, 27(7), 935-946.

21. Karunasena, W.M., Shah, A.H. (1991). Elastic Wave Propagation in Laminated composite Plates. Journal of Engineering Materials and Technology , 113, 411-417.

22. Kishimoto, K., Inoue, H., Hamada, M., Shibuya, T., (1995). Time Frequency Analysis of Dispersive Waves by Means of Wavelet Transform. Journal of Applied Mechanics 62 841-846.

23. Lee, P.C.Y., Chang, N., 1979. Harmonic Waves in Elastic Sandwich Plates. Journal of Elasticity, 9(1), 51-69.

24. Brillouin, L., (1960). Wave Propagation and Group Velocity. New York and London.

25. Lin, X., Yuan F.G., (2001). Diagnostic Lamb Waves In an Integrated Piezoelectric Sensor/Actuator Plate, Analytical and Experimental Studies. Smart Materials and Structures, 10, 907-913.

26. Michael, J.E., (1986). Determination of Dynamic Forces from Wave Motion Measurements. ASME Journal of Applied Mechanics, 53, 61-68.

27. Nayfeh, A.H., Chimenti, D.E., (1989). Free Wave propagation in Plates of General Anisotropic Media. ASME Journal of Applied Mechanics, 56, 881-886.

28. Noiret, D., Roget, G., (1989). Calculation of Wave Propagation in Composite Materials Using the Lamb Wave Concept. Journal of Composite Materials, 23, 195-205.

29. Park, H.C., Kim, D.S., (2001). Evaluation of the Dispersive Phase and group Velocities Using Harmonic Wavelet Transform. NDT & E. International 34, 457-467.

30. Prosser, W.H. and Gorman, M.R., (1994). Plate Mode Velocities in Graphite/Epoxy Plates. Journal of Acoustic Society of America, 96(2), 902-907.

31. Rao, J.S., (1999). Dynamics of Plates. Marcel Dekker, Inc., NewYork, Basel, Hongkong.

32. Timoshenko, S., (1940). Theory of Plates and Shells. McGraw Hill Book Company.

33. Timoshenko, S., Lessels, J.M., (1925). Applied Elasticity. Westinghouse technical night school press, East Pittsburgh, PA.

34. Soedel, W., (1993). Vibrations of Shells and Plates. Marcel Dekker Inc., NewYork, Basel, Hongkong.

35. Wu, T.T., Chen, Y.Y., (1999). Wavelet Analysis of Laser Generated Surface Waves in Layered Structure with Unbond Regions. ASME Journal of Applied Mechanics 66, 507-513.

36. Whitney, J.M., (1973). Shear Correction Factors For Orthotropic Laminates Under Static Load. ASME Journal of Applied Mechanics, 40, 302-304.

37. Yu, Y.Y., (1960). Forced Flexural Vibrations of Elastic Sandwich Plate. ASME Journal of Applied Mechanics, 27, 535-540.

38. Ziola, S.M., Gorman, M.R., (1991). Source Location in Thin Plates Using Cross-Correlation. J Acoustic soc Am, 90(5), 2551-2555.

39. Li, J., (2002). Intelligent Load Monitoring in Beam Structures. Master of Science thesis submitted to the faculty of the Department of Mechanical Engineering at North Carolina State University.

40. Mindlin, R.D., (1951). Influence of Rotary Inertia and Shear on Flexural Motions of Isotropic, Elastic Plates. Journal of Applied Mechanics, 18, 31-38.

41. Salehian, A., Hou, Z., Yuan, F.G., (2003). Identification of Location of a Sudden Damage in Plates Using Wavelet Approach. Submitted to 16th. ASCE Conference, University of Washington, Seattle.

APPENDIX A: RESPOSNSE SIMULATION AT SENSOR LOCATIONS

A.1: Isotropic Plate

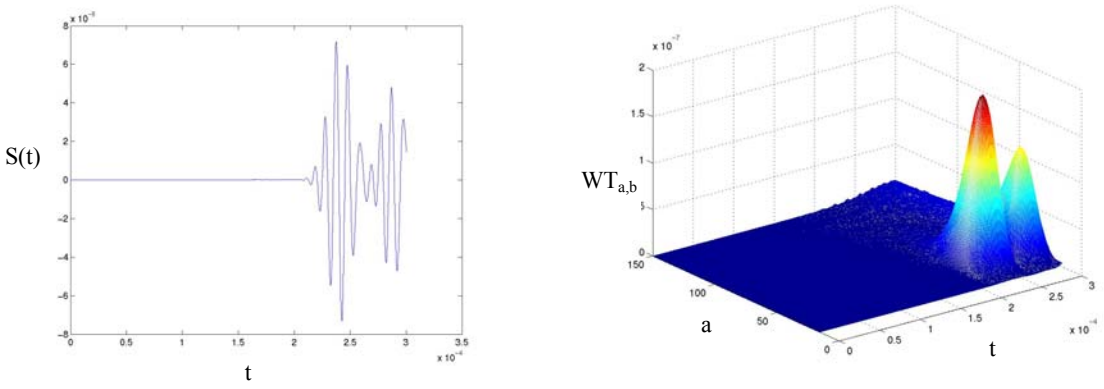

Figure A-1 Signal recorded at sensor 2 in isotropic plate for the narrow band load and the wavelet transform.

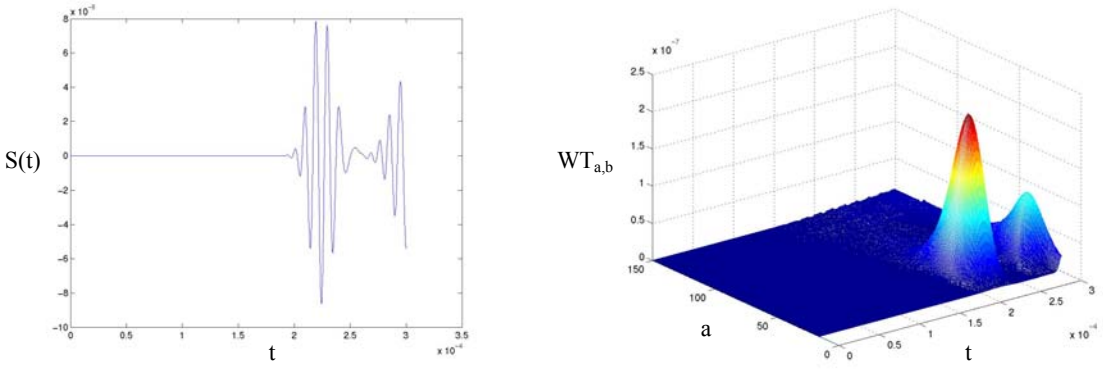

Figure A-2 Signal recorded at sensor 3 in isotropic plate for the narrow band load and the wavelet transform.

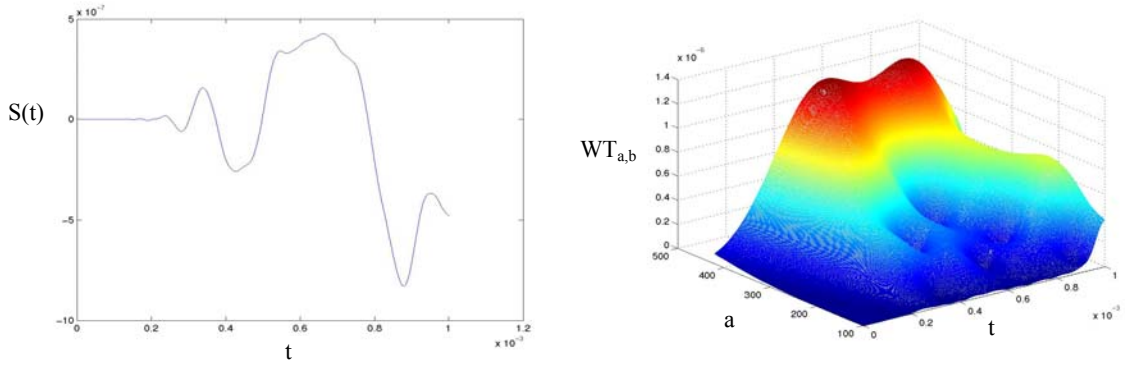

Figure A-3 Signal recorded at sensor 2 in isotropic plate for the wide band load and the wavelet transform

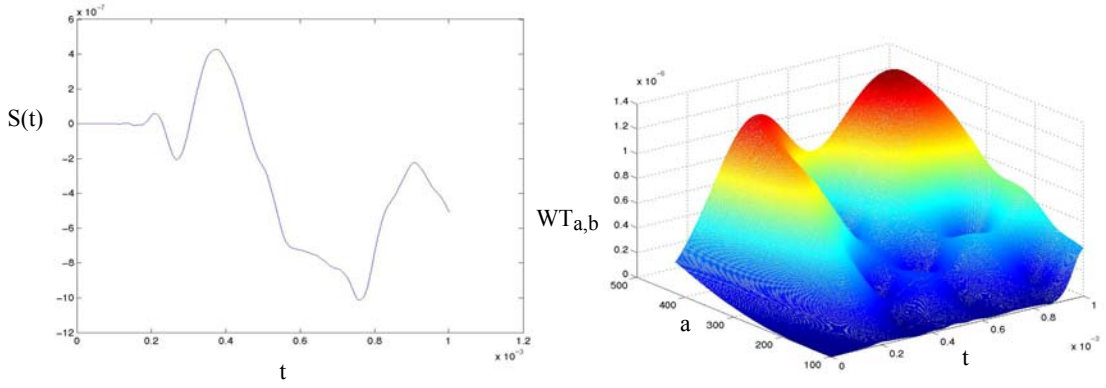

Figure A-4 Signal recorded at sensor 3 in isotropic plate for the wide band load and the wavelet transform

A.2: Composite Plate

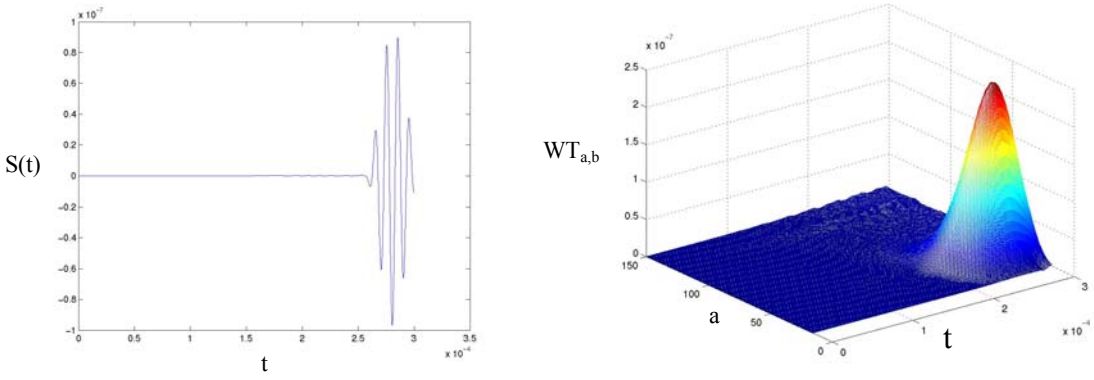

Figure A-5 Signal recorded at sensor 2 in composite plate 1 for the narrow band load and the wavelet transform

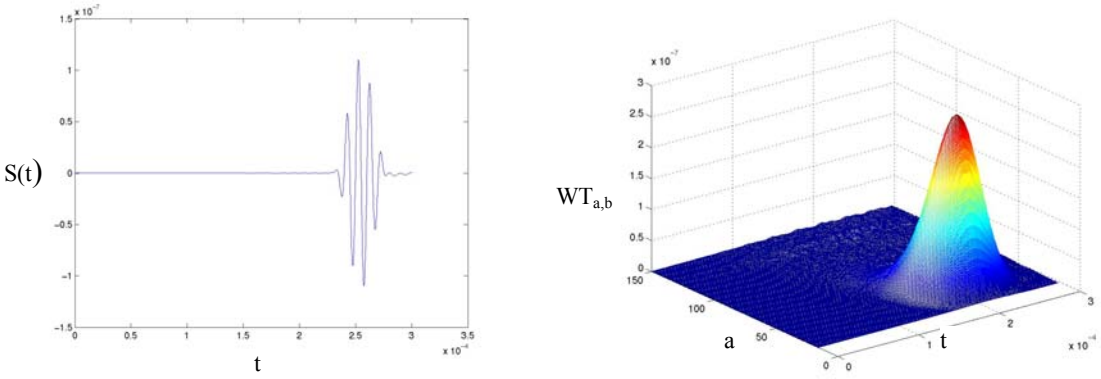

Figure A-6 Signal recorded at sensor 3 in composite plate 1 for the narrow band load and the wavelet transform

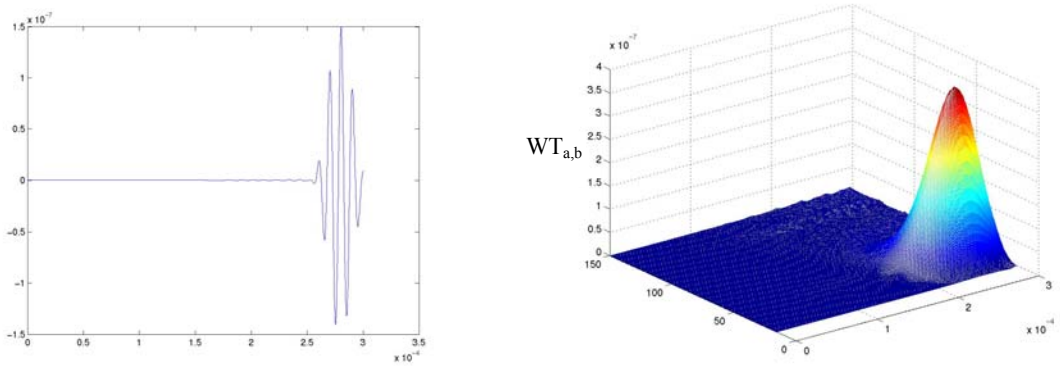

Figure A-7 Signal recorded at sensor 2 in composite plate 2 for the narrow band load and the wavelet transform

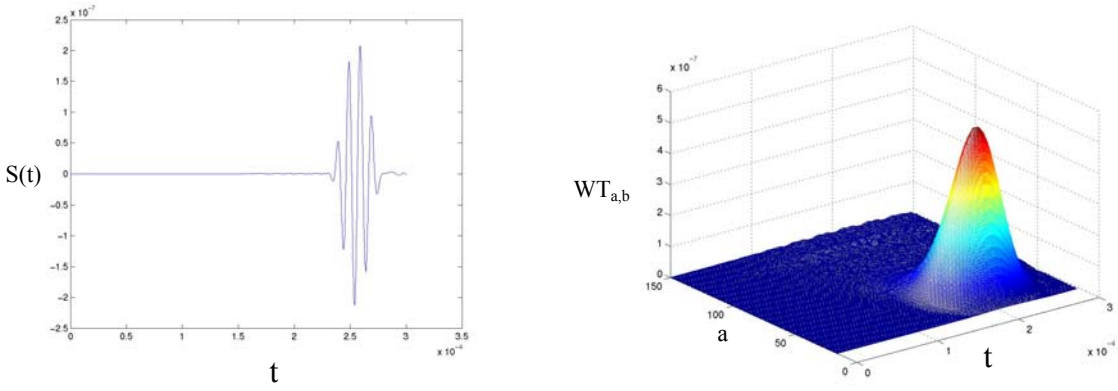

Figure A-8 Signal recorded at sensor 3 in composite plate 2 for the narrow band load and the wavelet transform

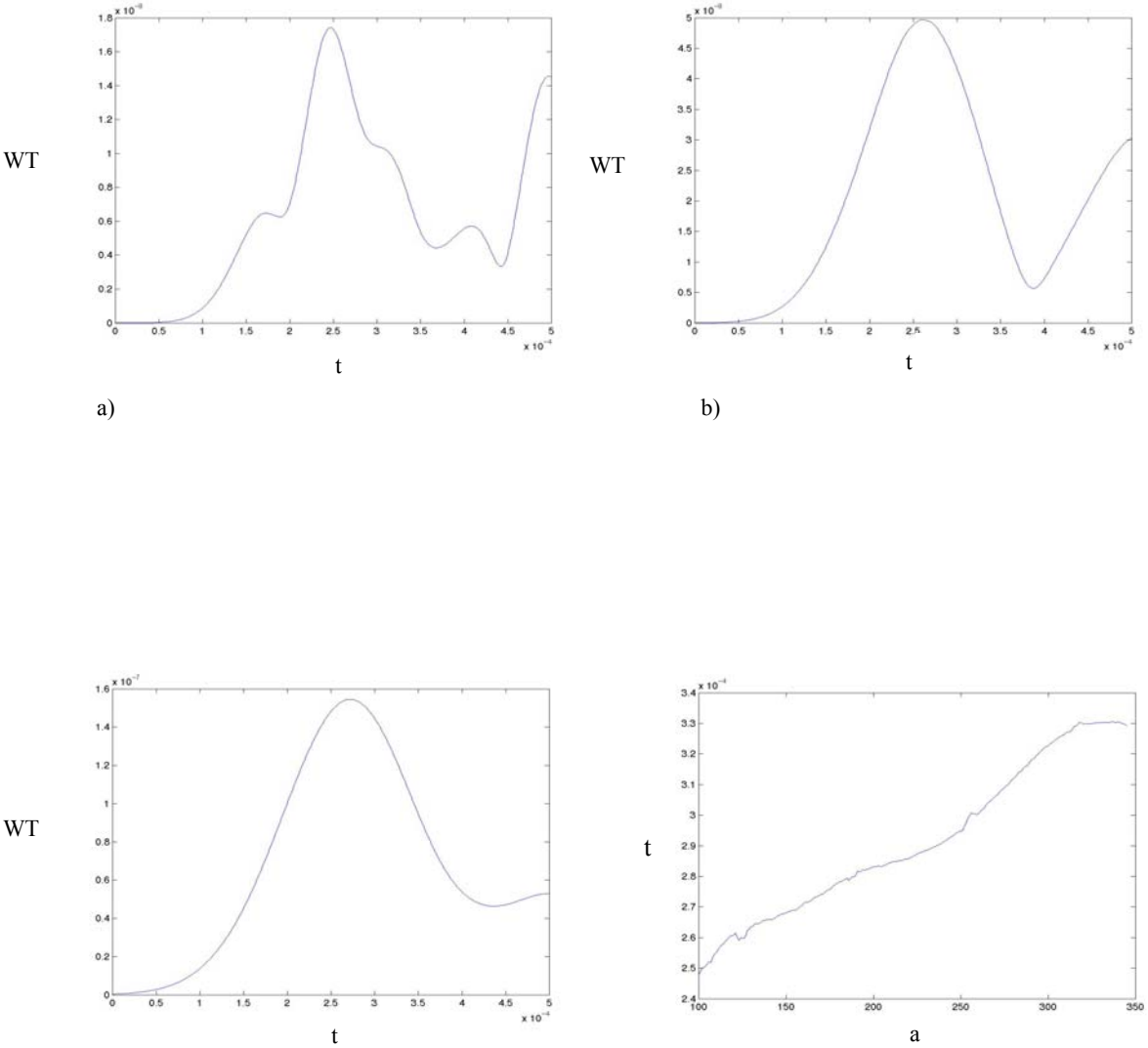

A-9 a) Magnitude of the WT for a= 100.53, f=39.8 KHz b) Magnitude of the WT for a=125.6, f=31.8 KHz c) Magnitude of the WT for a=167.55, f= 23.8 KHz d) Arrival time versus scale for sensor1in composite plate 1

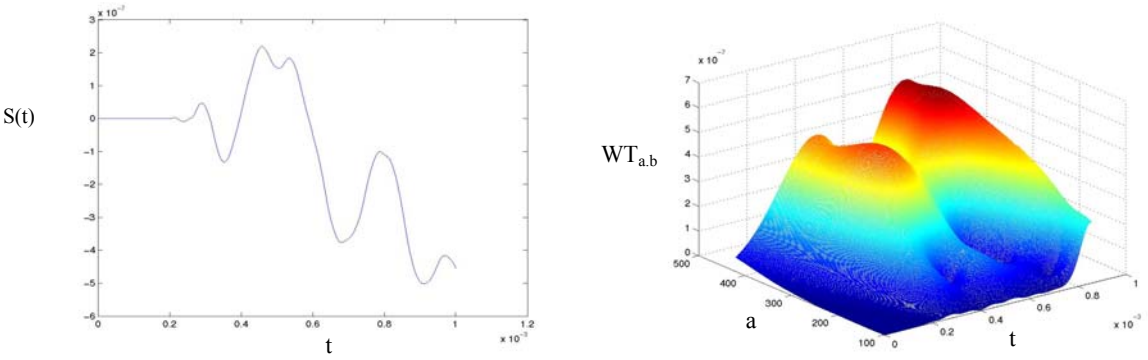

Figure A-10 Signal recorded at sensor 2 in composite plate 1 for the wide band load and wavelet transform

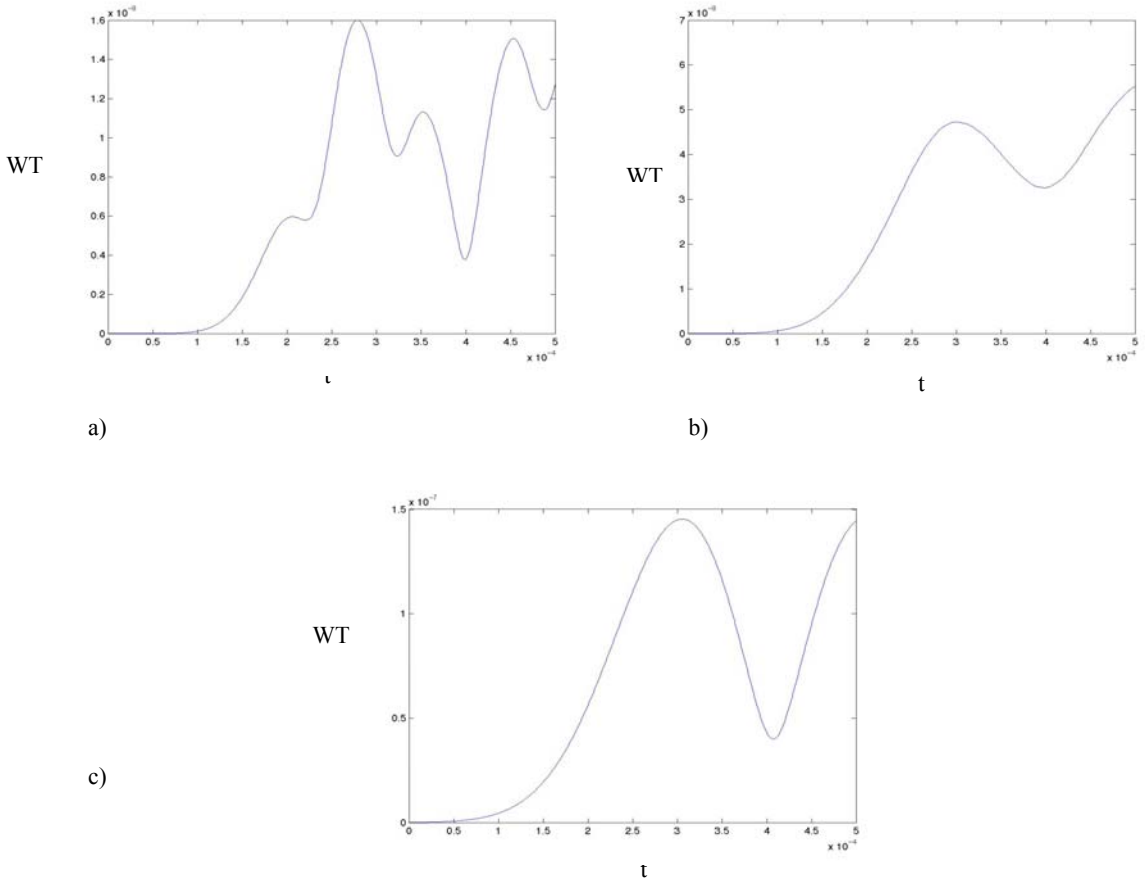

A-11 a) Magnitude of the WT for a=100.53, f=39.8 KHz b) Magnitude of the WT for a=125.6, f=31.8 KHz c) Magnitude of the WT for a=167.55, f= 23.8 KHz for sensor 2 in composite plate 1

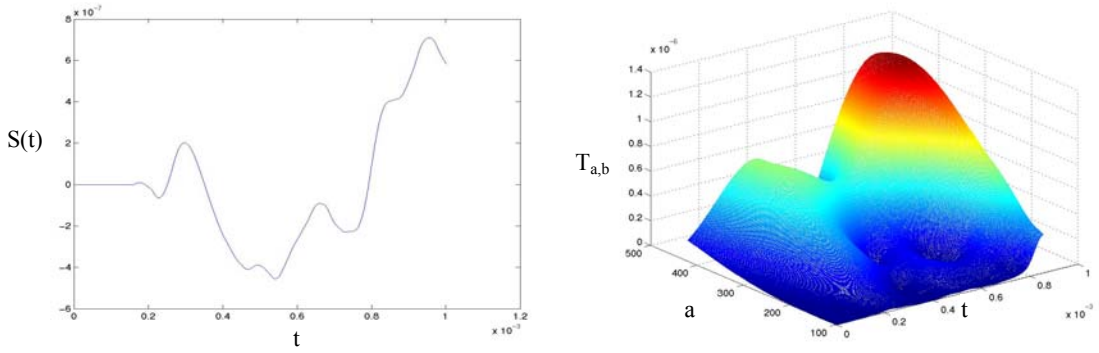

Figure A-12 Signal recorded at sensor 3 in composite plate 1 for the wide band load and wavelet transform

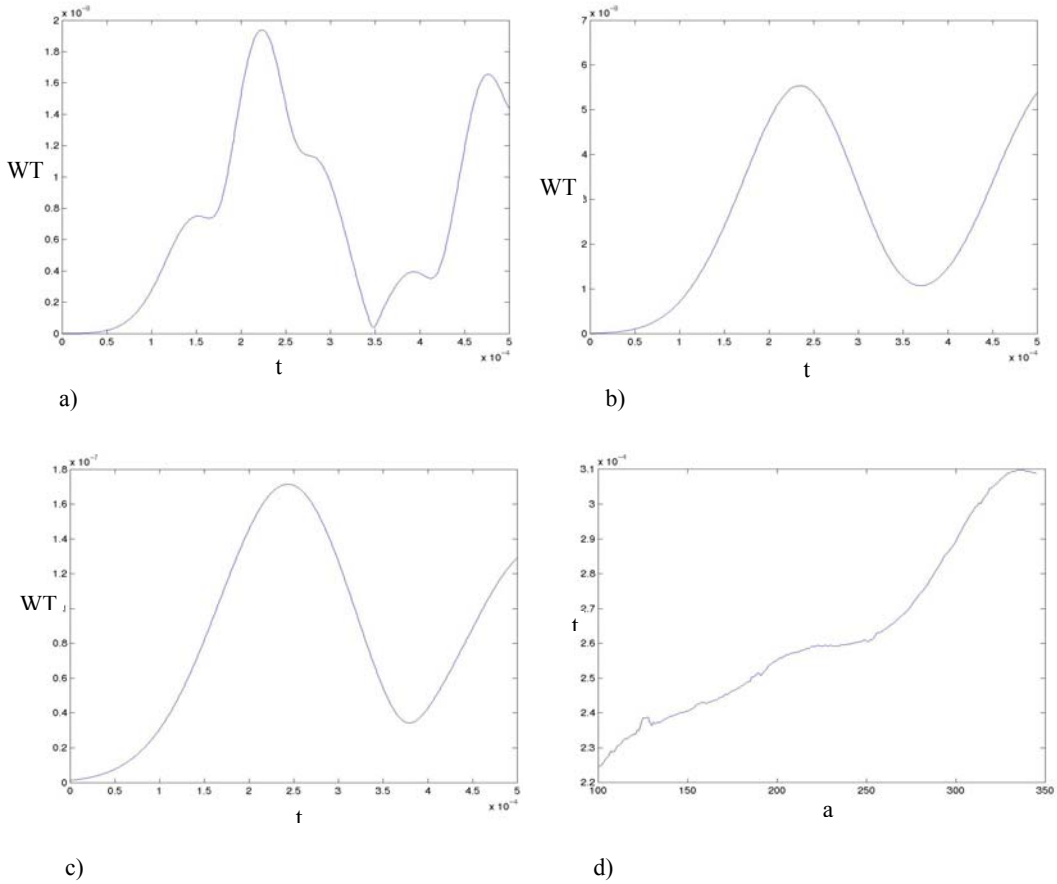

Figure A-13 a) Magnitude of the WT for a=100.53, f=39.8 KHz b) Magnitude of the WT for a=125.6, f=31.8 KHz c) Magnitude of the WT for a=167.55, f= 23.8 KHz d) Arrival time versus scale for sensor 3 in composite plate 1

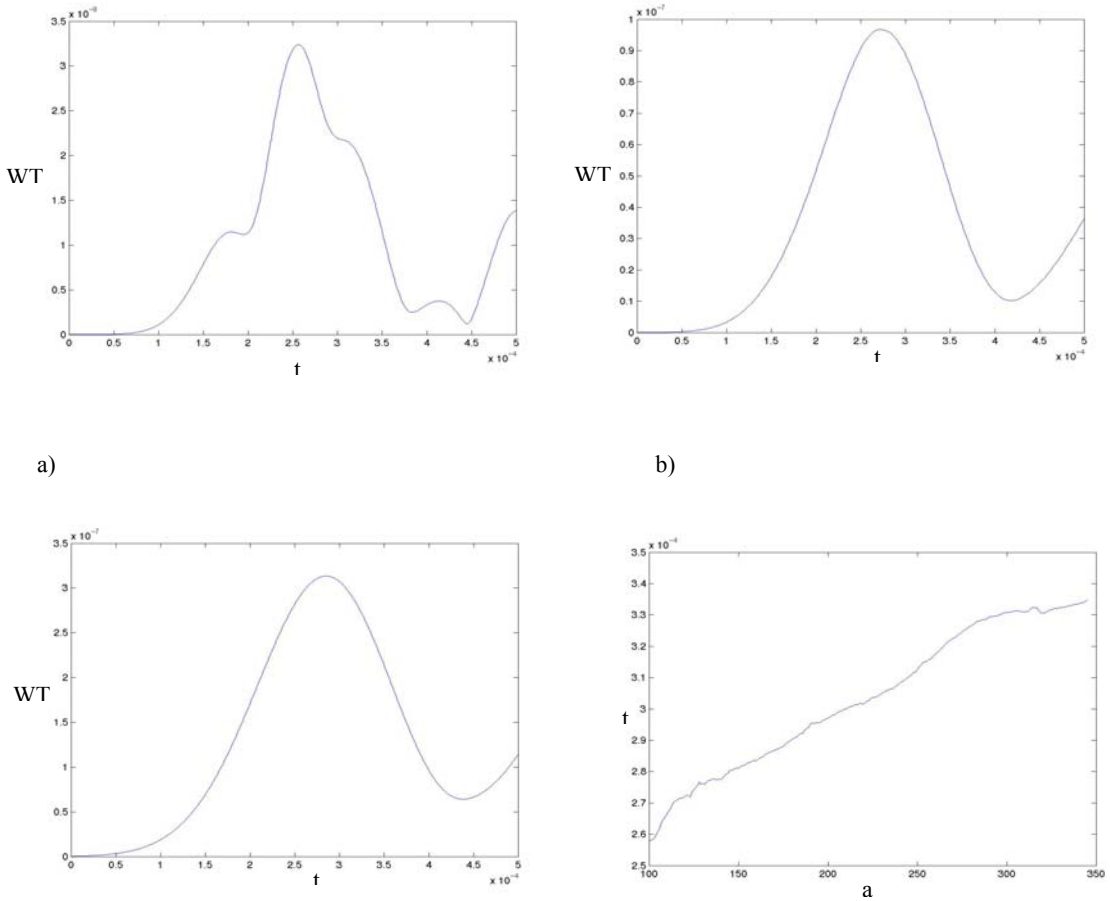

A-14 a) Magnitude of the WT for a=100.53, f=39.8 KHz b) Magnitude of the WT for a=125.6, f=31.8 KHz c) Magnitude of the WT for a=167.55, f= 23.8 KHz d) Arrival time versus scale for sensor 1 in composite plate 2

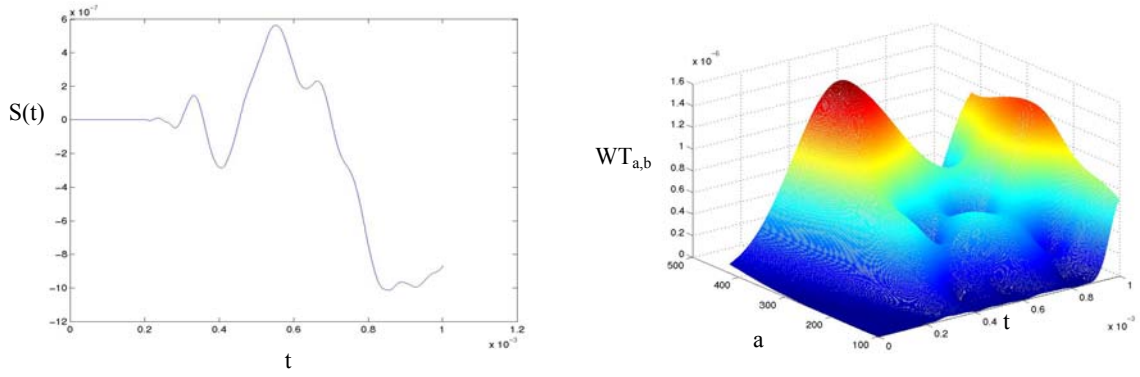

Figure A-15 Signal recorded at sensor 2 in composite plate 2 for the wide band load and the wavelet transform

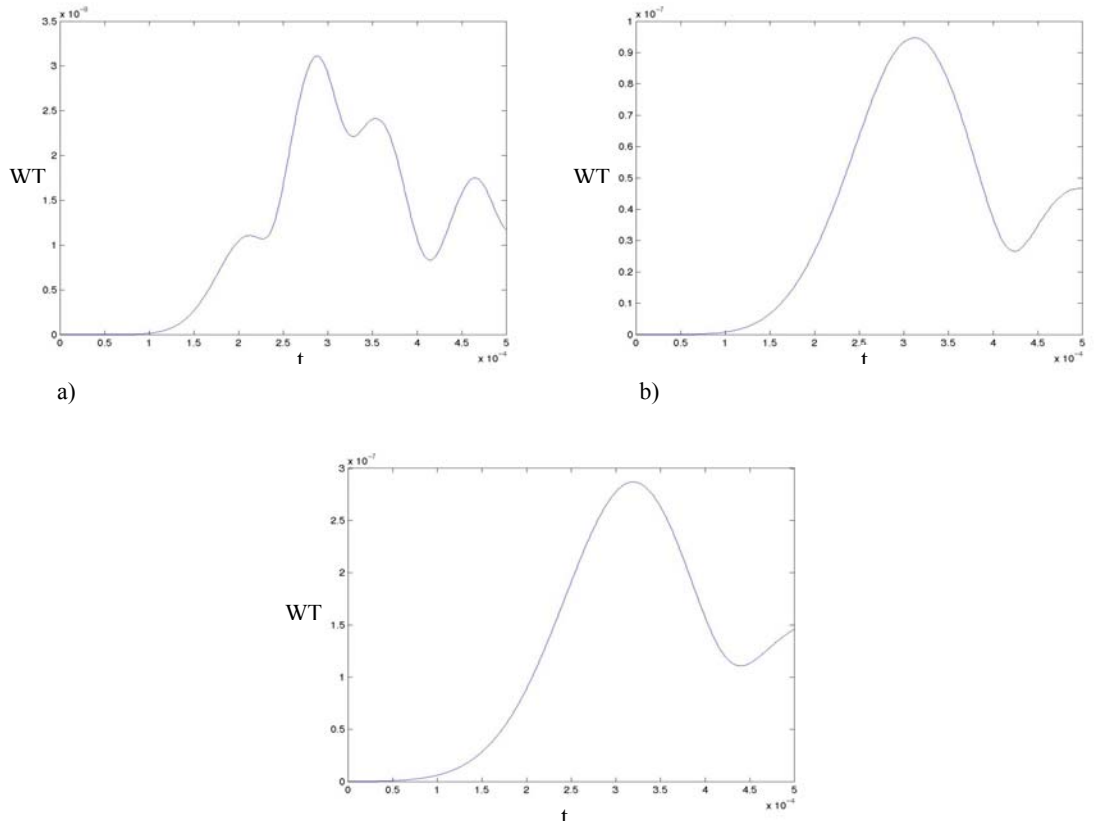

A-16 a) Magnitude of the WT for a=100.53, f=39.8 KHz b) Magnitude of the WT for a=125.6, f=31.8 KHz c) Magnitude of the WT for a=167.55, f= 23.8 KHz for sensor 2 in composite plate 2

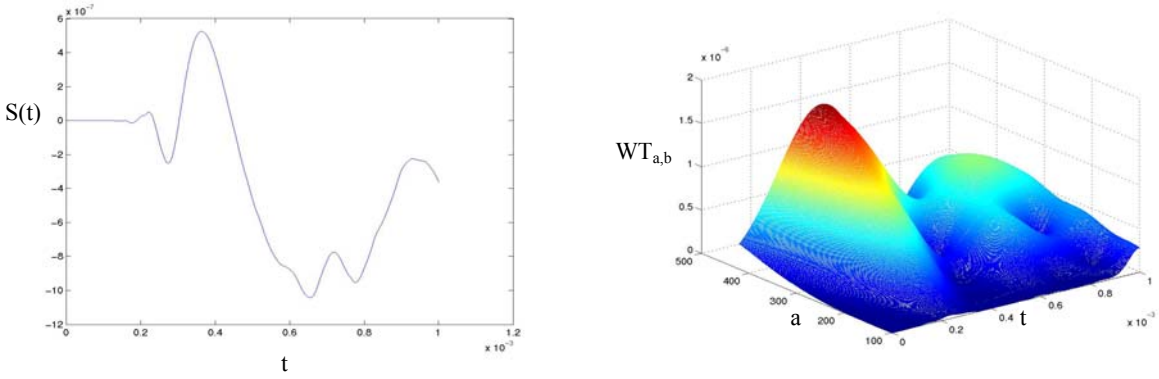

Figure A-17 Signal recorded at sensor 3 in composite plate 2 for the wide band load and wavelet transform

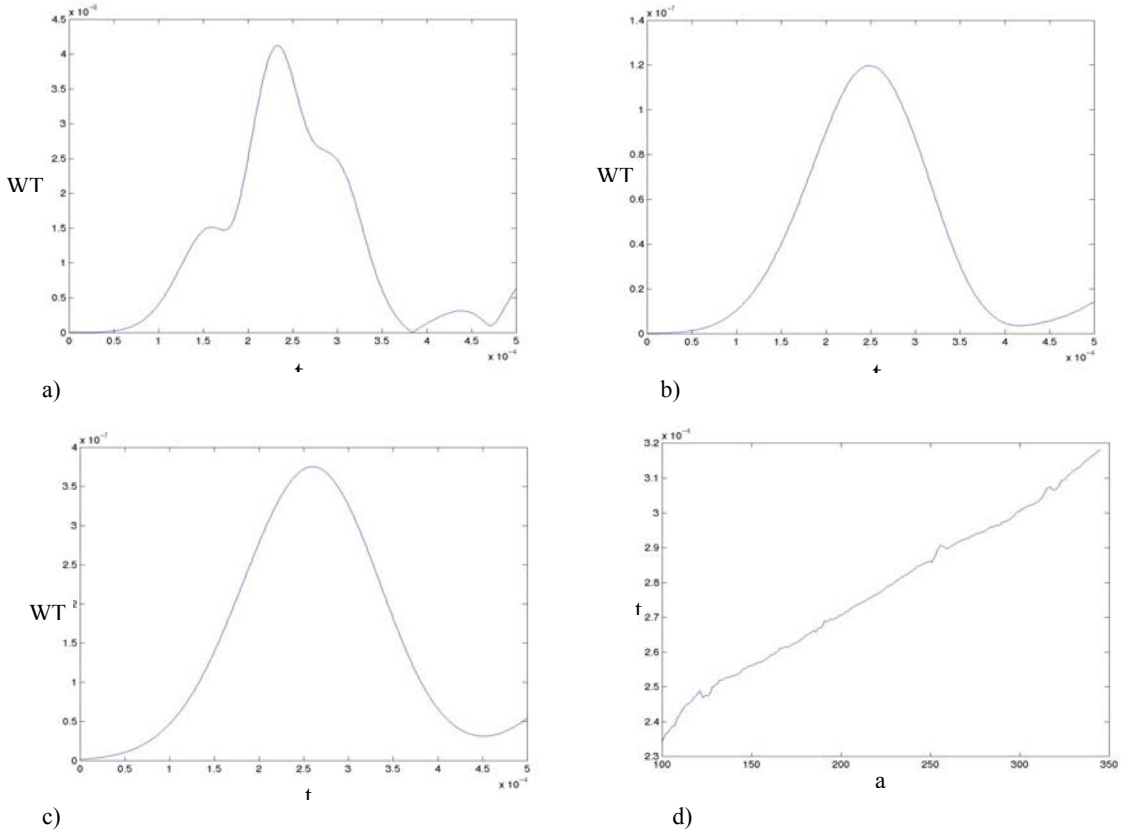

A-18 a) Magnitude of the WT for a=100.53, f=39.8 KHz b) Magnitude of the WT for a=125.6, f=31.8 KHz c) Magnitude of the WT for a=167.55, f= 23.8 KHz d) Arrival time versus scale for sensor 3 in composite plate 2

APPENDIX B: RESULTS FOR SIGNAL TO NOISE RATIO OF 15

Table B-1 Arrival times for different frequency Contents to sensors in composite plate-1 (10^{-4}sec.)

Noise	Noise level 7%-SNR 15		
Freq. / Sensor	23.8 (KHz)	31.8 (KHz)	39.8 (KHz)
S_1	2.625	2.495	2.73
S_2	2.96	2.785	3.05
S_3	2.28	2.24	2.41

Table B-2 Arrival times for different frequency Contents to sensors in composite plate-2 (10^{-4}sec.)

Noise	Noise Level 7%- SNR 15		
Freq. / Sensor	23.8 (KHz)	31.8 (KHz)	39.8 (KHz)
S_1	2.76	2.51	2.79
S_2	3.195	2.8	3.13
S_3	2.455	2.345	2.59

Table B-3 The coordinates found for the location of the applied load (m)

Noise / Location Found		Noise Level 7%-SNR 15		
		23.8 (KHz)	31.8 (KHz)	39.8 (KHz)
Composite 1	x	0.4985	0.5025	0.5025
	y	0.7099	0.7002	0.7002
Composite 2	x	0.4938	0.5022	0.5070
	y	0.7059	0.6936	0.6973